Master Thesis in Geographical Information Science nr 100

Investigating the accuracy of Digital Elevation Models from UAV images in areas with low contrast:
A sandy beach as a case study

Hemin Tofiq

2019
Department of
Physical Geography and Ecosystem Science
Centre for Geographical Information Systems
Lund University
Sölvegatan 12
S-223 62 Lund
Sweden

Hemin Tofiq (2019). Investigating the accuracy of Digital Elevation Models from UAV images in areas with low contrast: A sandy beach as a case study

Master degree thesis, 30/ credits in Master in Geographical Information Science
Department of Physical Geography and Ecosystem Science, Lund University

Investigating the accuracy of Digital Elevation Models from UAV images in areas with low contrast:
A sandy beach as a case study

Hemin Tofiq
Master thesis, 30 credits, in Geographical Information Sciences

Supervisor: Per-Ola Olsson
Department of Physical Geography and Ecosystem Science
Lund University, Sweden

Abstract

Elevation models are important in many applications in Geographical Information System (GIS), both when applying environmental analyses and in urban planning studies. The production of elevation models has been a difficult and expensive task using traditional surveying techniques. Remote sensing methods for producing digital elevation models have solved the difficult part of the task, which consist of collecting high resolution elevation data; however, the cost of elevation datasets has resulted in the fact that they have been among the least updated GIS datasets. Using Unmanned Aerial Vehicles (UAVs) is an effective and inexpensive approach for data collection that can facilitate the production of high temporal and spatial resolution elevation models. The method used for obtaining 3D models from overlapping images has been known for decades. Software that uses scale invariant object recognition methods to obtain 3D models from multiple images has been used both in computer vision and GIS applications. This study investigates the quality of elevation models obtained from images in areas with low elevation changes and low image contrast, i.e. coastal areas. The influence of image pixel size on the quality of the results is studied, as well as how the number and distribution of the Ground Control Points (GCPs) influence the accuracy of the models. The outputs of the study show a high correlation between pixel size and the quality of the obtained elevation models. While the number and distribution of the GCPs have a strong impact on the results, neither number of overlapping images nor different land cover types record a clear effect on the quality of the calculated GCPs. The difference between a number of elevation models express a systematic distribution of error with lower error values around the GCPs. The study demonstrates that time and resources can be saved and still obtain better results by selecting the best flight height with the optimal number and distribution of the GCPs.

Keywords: UAV, GCP, coastal monitoring, digital elevation model, Accuracy

Table of contents

List of tables

List of figures

1. Introduction:

The effect of climate changes, represented in a larger number and stronger storms during the last decades has caused substantial morphological changes in coastal areas (Taveira-Pinto et al., 2011). The necessity of monitoring these areas appears clearly when we know that 10 percent of the world's population and 13 percent of the urban population lives in areas lower than 10 meters above sea level (McGranahan et al., 2007). Hence, there is a major interest in efficient methods to monitor coastal areas.

Producing Digital Surface Models (DSM), which is one of the tools for monitoring coastal areas, has been the area of airborne Light Detection and Ranging (LIDAR) for several decades (Haala and Rothermel 2012). Other techniques that have been used in this area are Terrestrial Laser Scanning (TLS), GPS surveys, total stations and All Terrain Vehicle (ATV) (Turner et al., 2016). However, these traditional monitoring techniques have either low spatial resolution or high cost limitations.

One solution to these limitations is to take advantage of Unmanned Aerial Vehicles (UAVs) for coastal monitoring. Using UAVs in applications within the field of GIS is a hot topic in the community that works with spatial data. The main advantages of using UAV in coastal monitoring are low hardware cost compared to traditional surveying equipment, inexpensive and easy to operate, high level of automation of data acquisition (Goncalves and Henriques, 2015) as well as high spatial resolution. These features make UAV a reliable tool for applications that require a high temporal resolution.

The main challenges related to using UAVs in coastal areas are the weather conditions and water bodies present in the images. Strong winds can challenge the process of data collection, water bodies and moving objects must be masked out during data processing to prevent using them in the DSM production (Long et al., 2016). In addition, the process of DSM production in sandy surfaces is not an easy task due to the brightness of the sand and the low contrast in the images. Efforts to manage this challenge has been carried out through acquiring the images in the early morning with a low solar elevation and marine debris on the sand resulting in increased contrast and thus has been helpful in the process of point matching (Goncalves and Henriques, 2015). However, we do not find many studies that use UAV images for monitoring and analysing coastal areas (Goncalves and Henriques, 2015).

1.2 Research questions and Aims

The semi-uniform structure of sandy areas may challenge the process of finding corresponding points in a set of overlapping images. The aim of this study is to study whether it is possible to obtain DSMs from UAV images with qualities that can be compared to traditional surveying methods.

Specific research questions are:

- Analyze how pixel size of UAV images influences the quality of the obtained DSMs.
- Investigate the influence of number and distribution of GCPs
- Evaluate the effect of number of overlapping images
- How or whether the existence of other land-cover types affect the results.

2. Background

2.1 Monitoring coastal areas

The two main components of the surface of earth, water and land, meet at coastal areas. The form and the structure of coastal areas depends therefore originally on the interaction between these two components. The fact that a large number of the world's population live in coastal areas with low altitude above sea level, demonstrate the significant value of monitoring and detecting changes in these areas (Casella et al., 2016).

Changes in coastal areas are caused both by natural factors and human activities. Beside man-made factors, for instance removal of vegetation, deforestation, removal of sand for construction purposes and other kinds of human interventions (Mangor, 2018), coastal areas are affected by natural factors such as wave and tidal forces, winds, sediment and initial topography (Yoo and Oh, 2016). Important parameters that can be used in monitoring these changes is changes in the elevation and the volume of sand.

Applying ground-based surveying in coastal areas is associated with a number of challenges, among them, the difficulties related to the measurement process and the lack of ground control points and permanent objects that can be used as references. Other approaches that can be used to produce DSM with a high quality also have their limiting factors, for instance, the number of points to be measured using global navigation satellite system (GNSS), the long survey sessions when using TLS and the cost of using the LIDAR technology (Mancini et al., 2013).

Beaches have been traditionally monitored with total stations, GPS surveys, laser scanners and LIDAR. Despite their high accuracy, the main disadvantage of using these techniques is their high price levels, that make them insufficient for tasks that require frequent data collection. Another disadvantage is that the end product of these techniques will not contain an orthophoto, that can be used to study the terrain from other perspectives, for instance in monitoring changes in gain/loss of vegetation (Casella et al., 2016).

UAVs can help us in applying regular monitoring and better understanding the topography of coastal areas (Casella et al., 2016). One of the main benefits of using UAVs for monitoring coastal changes is the large amount of elevation data obtained via DSMs with a high spatial resolution, compared to traditional survey methods. Using high resolution data changes the quality of the elevation models resulting e.g. in more accurate estimates of volumes. Arango and Morales (2105) compared the accuracy of calculated volume obtained from UAV data with the traditional surveying method using total station and concluded that the estimated volume with UAV data is more accurate.

We can produce DSM using UAV with similar accuracies as the conventional LIDAR, both airborne and terrestrial (Long et al., 2016). The spatial resolution of the produced models depends nevertheless on the flight height and the sensor/camera specifications. A number of studies (Raeva et al., 2016; Stalin and Gnanaprakasam, 2017; Zylka, 2014) concludes that the UAV images have the potential to be considered as a competitive method both in comparison with traditional surveying techniques, GNSS based or LIDAR methods for producing digital elevation models and volume calculation.

2.2 UAV data collection

The main components used in topographic surveying with UAVs consist of the UAV airframe, equipment for measuring Ground Control Points (GCPs) with high accuracy and software to be used for processing UAV images. The UAV airframe incorporate the data acquisition unit which consists of a digital camera and in some cases a thermal, spectral or any other lightweight sensor. The next sections describe the three main components of UAV data collection and circumstances that must be taken in to account when using UAV in coastal areas.

2.2.1 UAV data collection in coastal areas

UAVs is a cost-effective way of surveying in coastal areas, especially when using autonomous flight techniques and survey-grade GPS, which eliminates the time intensive process of on-ground surveying GCPs (Turner et al., 2016). Survey-grade GPS, compared to recreational and mapping GPS receivers are the most accurate receivers (eXtension, 2014). UAVs have been used in many projects and several GIS applications; however, we find only few studies related to using UAVs in coastal monitoring (Goncalves and Henriques, 2015).

One main challenge related to using UAV in coastal areas is the weather conditions. Therefore, it is important to take advantages of the periods with low wind, especially early mornings. Another challenge is the existence of water bodies in coastal areas, these areas must be masked out before using the images, to prevent using them in the point matching process. It is also important to be aware of the time of the day where there is low tide, so that the largest coastal area is mapped.

UAV images should generally be captured in cloudy skies to avoid shadows in the image (Casella et al., 2016). The technique used for DSM production relies mainly on feature identification which is apparently not an easy task due to the brightness of the area and the low

variation of the surface and the low contrast of the objects in the images. One of the methods to deal with this challenge is to perform data collection in the early morning with a low sun and marine debris on the sand to get as much contrast as possible (Goncalves and Henriques, 2015).

2.2.2 Georeferencing and Ground Control Points (GCPs)

Ground control points are important for precise georeferencing of images in the process of DSM creation. High accuracy measurements of a number of GCPs in the study area is required to georeference the models that will be obtained in the data processing steps.

Real Time Kinematic (RTK) positioning with an accuracy of 1-2 cm can be used in surveying ground control points. It is important to be aware that the GPS pole can easily go through the sand surface when collecting data in coastal sand areas; this will influence the accuracy of elevation data.

Long et al. (2016) concluded that it is important to have GCPs located in the corners and in the center of the study area in a homogeneous distribution. Having a GCP for about every 250 meters has been one of the requirements for obtaining a DSM with a high accuracy. Increasing the number of GCPs decreases the vertical difference; however, the vertical difference, according to their study, remains unchanged when it reaches 9 cm, i.e. using more than 14 GCPs in an area of 75 ha do not result in DSMs with lower vertical error values than 9 cm. The study carried out by Long et al. records only a slight influence of the pixel size on the obtained results. Considering and excluding water surfaces before data processing is one of the recommendations of the study and apparently one of the error sources.

A project carried out by Turner et al. (2016) emphasizes the advantages of using RTK-GPS for positioning the camera location at capturing time and concludes that combining the camera position with the redundancy of the image overlaps, will make ground surveys for GCPs unnecessary, which is a time-consuming process, generally, and a more difficult task in coastal areas.

RTK GPS onboard UAVs will have advantages in coastal areas since the data-link connection will be stable, thus most of the images will have well corrected locations, opposite to urban areas where Post Processed Kinematic (PPK) may be required and the images most likely end up with uneven weighted camera location qualities. In a comparison between RTK GPS onboard UAVs and GCPs Chen (2017) concluded that DSM with 1 Ground Sampling Distance (GSD) error in elevation can be obtained from RTK GPS onboard UAVs in open areas, while well distributed GCPs result in the best output in urban areas. RTK GPS onboard UAVs is especially advantageous when there is dense vegetation, crops or where it is not feasible to measure GCPs

due to safety concerns, even though cost of equipment and software that can handle different weighted camera locations are parameters we have to take in to account.

2.2.3 Structure From Motion (SFM)

Structure From Motion (SFM) is a method used for calculating the 3D locations of features from multiple overlapping images through identifying the features in a system that is invariant to scale and rotation (Westoby et al., 2012). SFM uses the same principles that are used by traditional stereoscopic photogrammetry, i.e. 3D models construction from a number of overlapping images. However, the main difference between SFM and ordinary photogrammetry is that SFM calculates camera locations and orientations by using an iterative process based on a set of features extracted automatically from the images (Snavely, 2008).

The first step performed by SFM is identifying a number of features from a set of images by using the Scale-Invariant Feature Transform (SIFT) algorithm (Westoby et al., 2012). SIFT allows matching corresponding features from multiple images even with variations in viewpoint, scale and changing illumination (Lowe, 1999). Having the location of two features on a minimum of two images, we can determine camera locations, orientations, focal lengths and relative location of these two features in a single step known as “bundle adjustment” (Nissen, 2016). Figure 1 shows the parameters used in SFM.

The output of the bundle adjustment step is a three-dimensional sparse point cloud. This output is then used by the MultiView Stereo (MVS) algorithm to produce a dense point cloud by using the calculated camera positions and SFM points (Westoby et al., 2012).

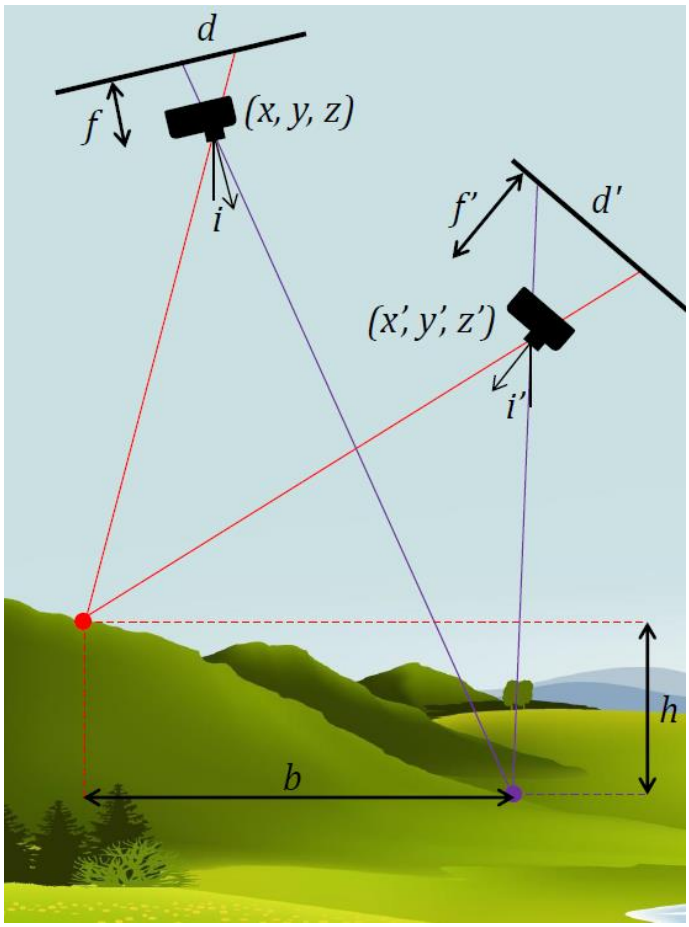

Figure 1. Structure From Motion (source Nissen, 2016)

A required step to georeference the 3D model created in SFM is the process of georectification, which means converting the obtained point cloud from an internal, arbitrary coordinate system into a geographical coordinate system by using camera positions and focal lengths or GCPs (Nissen, 2016; Westoby et al., 2012).

One of the popular software that has implemented SFM is Agisoft Photoscan[1], which is used in this project; however, other commercial software like pix4d[2] and open source software like OpenDroneMap[3] are also available.

[1] http://www.agisoft.com/
[2] https://pix4d.com/
[3] http://opendronemap.org/

2.3 DSM quality assessment, UAV versus traditional surveying techniques.

Assessing the DSM quality is a complicated task, especially when the DSM is obtained using UAV images due to the diversity of error sources. The main two error sources are the error in the GPS measurements that we use to in georeferencing the model and software error when warping the DSM (Mancini et al., 2013).

Comparing the measurements obtained monthly using ATV surveys with data produced from UAV images, the main benefit of the UAV surveying approach is the high spatial resolution of the point cloud achieved, with centimetres between the points, while low-density data need to be interpolated to be able to compare the obtained results with high density data from other sources. Turner et al. (2016) demonstrate that the differences between the two methods, ATV and UAV, are normally distributed with a mean difference of 2.6 cm that is perhaps related to the minor sinking effect of the ATV in the sand. The paper concludes that using UAVs for topographic surveying and mapping in coastal areas is an efficient and cost-effective approach.

Other works have been implemented to compare the quality of elevation data obtained from UAV images with results from TLS approaches and data produced by using GNSS survey. Mancini et al. (2013) have obtained an average error in centimeter level in terrains with a continuous structure, while larger values are observed in areas with sudden changes in terrain. The paper concludes that UAV provides a straightforward method for producing DSM with elevation accuracy that is comparable with results achieved by using the TLS approach.

Long et al. (2016) recorded results with low vertical error values, taking into account that the results are obtained from photogrammetry, they conclude that the average accuracy obtained by using UAV matches or exceeds the accuracy obtained with the conventional aerial photography. The same study has analyzed the effect of the numbers of GCPs on the quality of the generated DSMs and concludes that using UAV images, DSM with similar accuracies as the conventional LIDAR or TLS (Long et al., 2016) can be obtained.

The high number of overlapping images obtained from UAV data has substantial advantages for the dense cloud process and reconstruction of the surface model (Haala and Rothermel, 2012). This is a major advantage of UAV created elevation models compared to traditional surveying methods.

3. Methodology

This chapter is dedicated to defining the requirements and describing the preparations for data collection, processing of UAV acquired images and the approach used to answer the research questions.

3.1 The study area:

The study area is the upper part of the coastline at Ängelholm city in southern Sweden (Figure 2 and 3), The area is about 400 meters long and 20 to 40 meters wide, less wide at the north part. The coastline is nearly 6 kilometers of sandy beach in total. The beach is one on the main attractions in the municipality, close to a residential area and other social and commercial activities and therefore of a great interest for monitoring.
The coastline is mainly covered by sand. The eastern side of the beach is covered by bushes, sparse vegetation and rocks; therefore, we will also study how or whether vegetation and other land cover types influence the quality of the obtained DSMs.

The extent of the area in WGS84 and EPSG:3006 SWEREF99 TM) is:
Lower left: 12° 50' 10", 56° 16' 1" / 366000, 6237899
Upper right: ,12° 50' 18", 56° 16' 17" / 366148, 6238395

Figures 2, 3 and 4 show the location of the study area from different scales and sources.

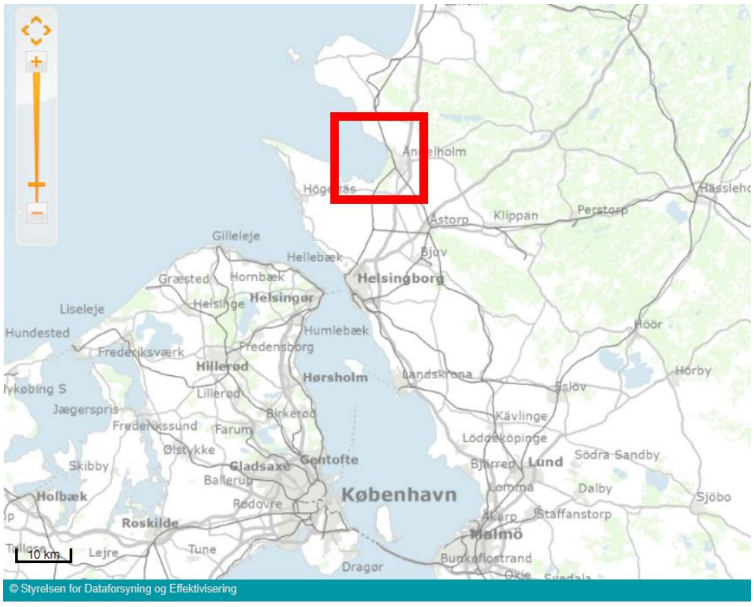

Figure 2. The study area in southern Sweden. Source: Geodatastyrelsen (www.gst.dk).

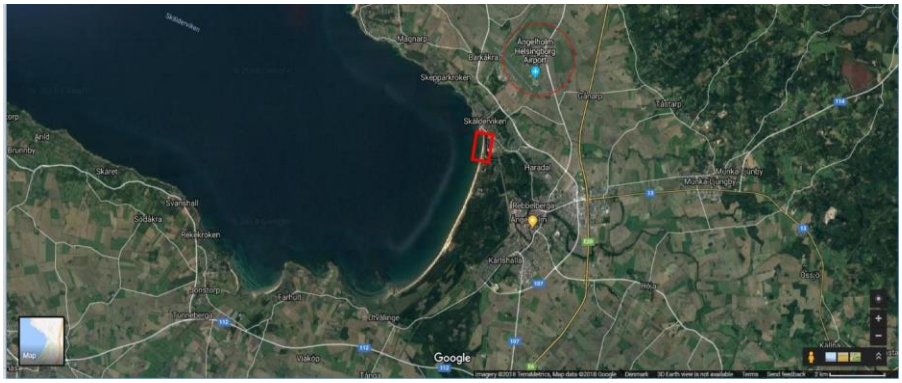

Figure 3. The study area, the upper part of the coastline at Ängelholm. Source: Google

Figure 4. The northern part of the beach, a view at the end time of data collection. Approved for publication, LM2018/002559.

3.2 Data collection:

This section describes shortly the necessary equipment used for data collection, fight planning and the two data sets used in the project, namely ground control measurements and UAV images.

3.2.1 Equipment

The UAV used for data collection was a 3DR Solo Quadcopter, i.e. it has 4 motors, capable of vertical take-off and landing and supports autonomous flight modes. The UAV was equipped with a PeauPro82 3.97mm (22mm) f/2.8 GoPro Hero 4 Black[4] camera and used to capture

[4] Hero 4 https://www.peauproductions.com/products/peaupro82

images with 8-bit depth in JPEG format and 4000 x 3000 pixels. The UAV and the camera is shown in figure 5.

Figure 5. HERO4 camera on board of the 3DR Solo UAV.

After UAV data collection, ground data collection was carried out with RTK GPS+GLONASS. A GPS of type Topcon and an RTK service from SWEPOS, the national service in Sweden were used. A total of 12 GCPs were measured. The observations were collected in the Swedish national reference system SWEREF99 TM and SWEN08-rh2000 geoid.

3.2.2 Flight planning and UAV data sets

The flight routes were designed using the Mission planner[5] software to capture images with 80% overlap forward and 70% side overlap and carried out with a speed of 5 meter per sec. Figures 6 and 7 are captured during planning and performing one of the missions.

Figure 6. Planning UAV flight sessions

[5] http://ardupilot.org/planner/

Figure 7. The 3DR Solo UAV at the time of performing one of the missions. Approved for publication, LM2018/002559.

To compare the influence of spatial resolution, a total of three flight sessions at 20, 30 and 40 meters flight height were designed and carried out in the study area resulting in GSD values shown in table 1.

Table 1. Flight heights and ground sampling distances.

Flight no.	Height (m)	GSD (cm)
1	30	1.14
2	20	0.79
3	40	1.51

As any other project where UAV is used for data collection, performing a flight session require flight planning and flight control. It is also important to be aware of the regulations related to using UAVs in the study area to ensure a safe and a proper use of UAVs both in regard to people in the area and their properties, but also to other flying objects.

Planning the day and the time for data collection required coordination with the municipality and Ängelholm Helsingborg airport because the study area lies within the flight control zone of the airport. The first hours of the 15. of May 2017 was unfortunately very misty, and thus we decided to have flights at low flight heights. The study area at the start time of data collection is shown in figure 8.

The mist disappeared, and it was completely clear at the end part of the time window agreed with the airport. The advantage of cloudy weather when collecting UAV data is the absence of sun, which prevents having shadows in the images that can affect the process carried out for creating DSMs. Another noteworthy point is the creation of water droplets on the sand which will give a better contrast in sandy areas and will help the software in finding unique features, it is therefore recommended to perform UAV data collection in coastal areas early in the mornings (Goncalves and Henriques, 2015).

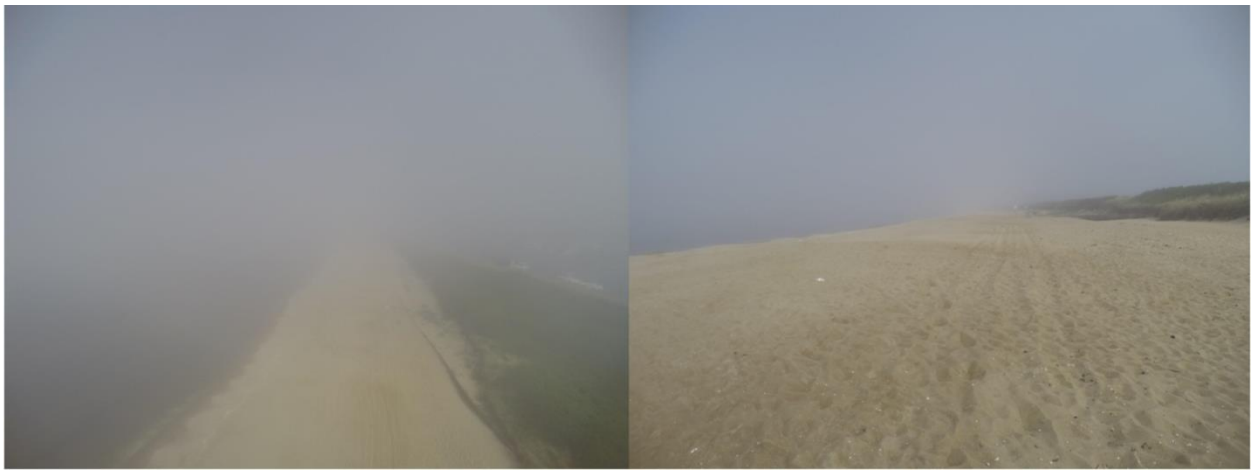

Figure 8. The study area at the day of data collection; very misty at the start time, clearer at the end of the time window agreed with the airport. Approved for publication, LM2018/002559.

Water bodies and moving objects must be masked out to avoid using these areas during the point matching process. Masking the water bodies is a time-consuming process, therefore it is relevant to take this point into account, as much as possible, when planning the flight route. In our case, the flights were controlled, and the drone returned home at the last part of the missions where we could see only images of the water bodies will be captured.

The flights were designed to be carried out along the beach and a larger area than the study area was captured to avoid having blurred images when the UAV turns at the end of the flight lines. Images outside the study area and images that only contain water bodies must be excluded before processing. The number of overlapping images were analyzed and their effect in relation to flight heights were investigated, since insufficient image overlap may result in holes in the models.

3.2.3 Ground control points

Pieces of white cloth (50cm x 50cm) with a black painted cross mark of 2 cm thickness were used as GCPs. Piece of cloth were used instead of a hard material so that it could follow the sand surface to get a more accurate measurement of the points and the surface of the area The GCPs were secured on the sand by using skewer pegs and partly covered by sand.

To recognize the artificial GCPs from the UAV images, a numbering system both as numbers and as a dot indicating the short hand in a clock was used, since it was expected that the numbers would not be clear in some of the images, then we could use the location of the dot to recognize the GCP. To indicate numbers above 12 an extra dot at 12 was added. The numbers were always written at the upper left of the cross sign. Figure 9 shows an example of the artificial GCP used in the missions and how it appears in flight 2 at 20 meters flight height. The numbers were not always clear, but the location of the dot, the clock numbering system, helped in recognizing the GCPs.

Figure 9. The artificial GCP, at the preparation time and from one of the flights.

The approximate locations of the GCPs were designed before flight start, both for the GCPs planned to be used in creating the models (control points)[6] and the GCPs that were used to evaluate the quality of the obtained models (check points). The artificial GCPs were distributed in the study area before starting the flight sessions. After collecting UAV data, the 12 GCPs were measured using Real Time Kinematic (RTK) GPS+GLONASS. The accuracy of the point measurements was 1-2 cm (horizontal and vertical). The GCP locations were saved and used in SWEREF99 TM coordinate system (EPSG:3006) and SWEN08-RH2000 geoid. When measuring the location of the ground control points, a small block of wood was used to avoid that the pole force itself through the sand. The height of the block was 1.9 cm which was subtracted from measured GCPs heights before using them in Agisoft PhotoScan.

[6] Applying the same terminology used by Agisoft, GCPs used in georeferencing the models will be referred as control points and GCPs used to evaluate the quality of the obtained models as check points.

3.3 Data processing

Processing the UAV data required defining the methods and the software used in the processing stages to obtain the required outputs and carry out the analysis. The software used for processing the UAV images was Agisoft PhotoScan, version 1.4.1. The main steps applied by Agisoft PhotoScan for processing the images and producing DSM and orthomosaic images of the study area were applied with high quality settings.

3.3.1 UAV data processing for DSM generation

Digital elevation model is one of the outputs obtained from UAV data processing in Agisoft PhotoScan. Using the software and implementing the processing steps for producing DSM and orthophotos is straightforward, since the steps are listed under a workflow, where it is not possible to perform a step before the requirements of the step are available, however, obtaining high quality results require image quality assessment, placing GCP markers, masking water bodies and other manual steps shown in figure 10.

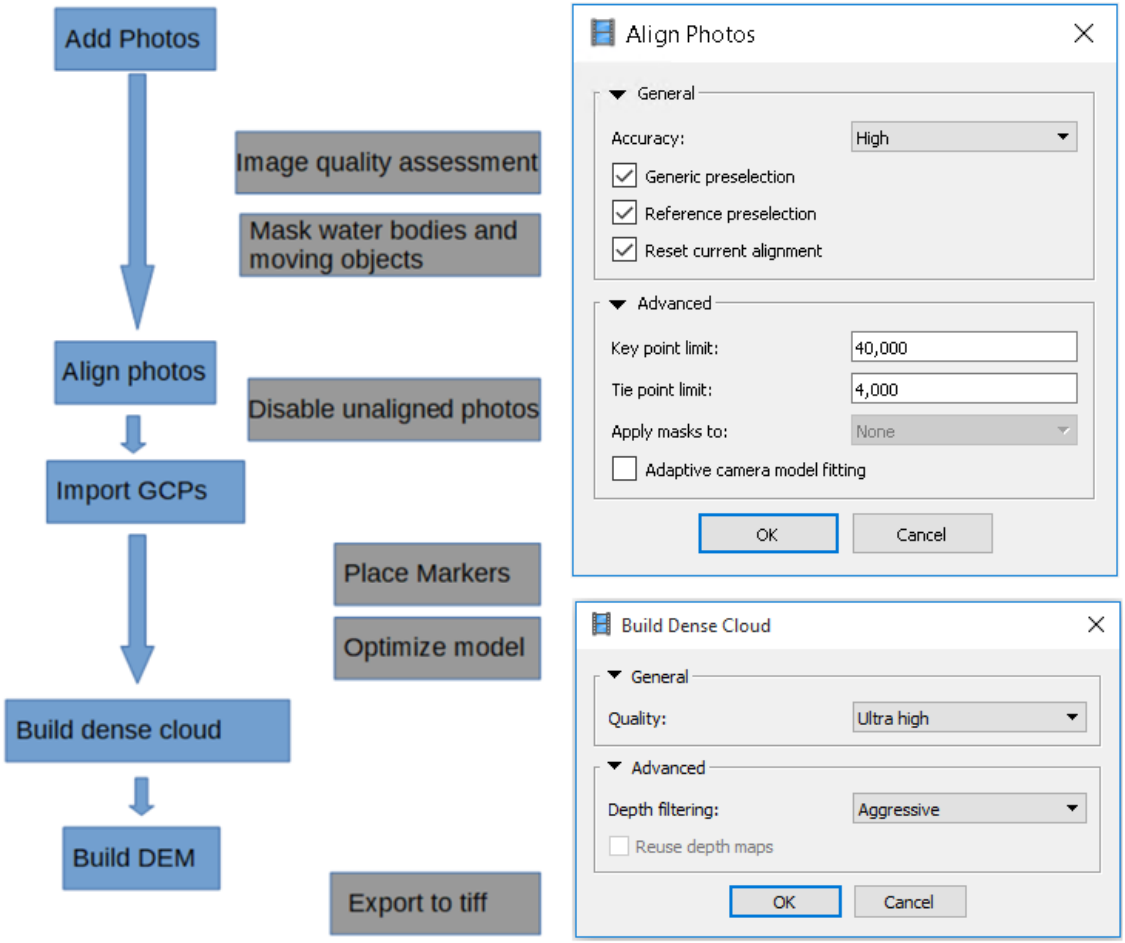

Figure 10. Data processing workflow for DSM creation and applied Agisoft PhotoScan settings

Some of the known challenges when working with UVA images is blurred images due to wind effects or other error sources. Blurred images must be excluded from the dataset. Images that cannot be aligned by the software must be disabled in the next processing steps.

Before running the alignment process, the quality of the images was verified. Agisoft PhotoScan provides a tool for estimating the quality of the images before using them in photogrammetric processing and recommends only using images with a quality unit of greater than 0.5. Images with a quality computed to less than this limit are classified as poor input and recommended to be disabled. The quality attribute in Agisoft PhotoScan is estimated from border sharpness and provides information about sharp borders in an image (Agisoft LLC, 2016). It is therefore expected to have images below the recommended values in flight 1 and 2, where the weather was misty.
Masking water bodies was carried out for all the three datasets before performing the required steps, which consists of alignment of the photos, creation of the dense cloud and building the elevation models.

3.3.2 DSM quality assessment

To be able to compare DSMs obtained from different flight sessions with various number and distribution of GCPs, the collected data sets were processed using Agisoft PhotoScan with the same quality settings. The workflow for obtaining DSMs from different number and distributions of GCPs is described below:

Based on number of GCPs:

To study how the number of GCPs influences the quality of the obtained DSMs, UAV images were processed with different numbers of GCPs, the same 4 to 8 GCPs were used with the three datasets. This procedure resulted in 15 DSMs, 5 for each flight session. A diagram demonstrating the processing steps for a UAV dataset is shown in figure 11.

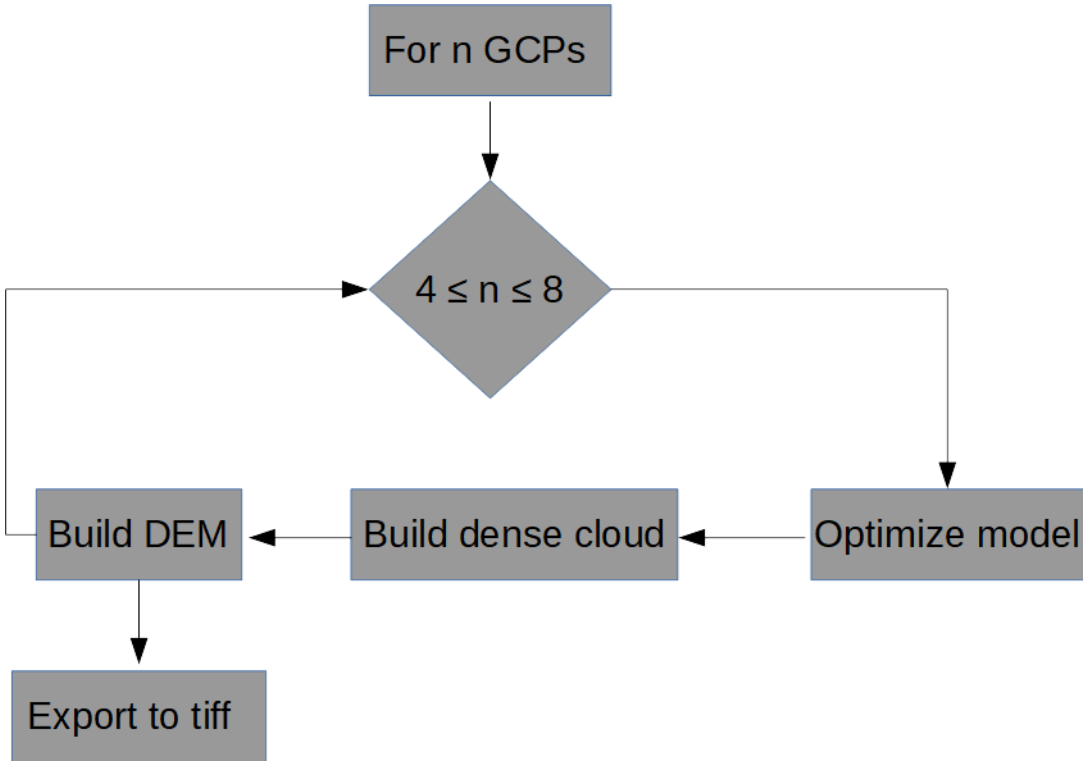

Figure 11. Creating DSMs with different number of GCPs.

Based on distribution of GCPs:

To study how the distribution of the GCPs influence the quality of the obtained DSMs, two other sets of DSMs were used. One set of 4 DSMs with different combinations of 4 GCPs and one set of 3 DSMs with different combinations of 6 GCPs. These combinations contain GCP sets that are distributed homogeneously, zigzag shaped, concentrated in the middle and the ends of the study area. The procedure used for creating DSMs from different distribution of 4 and 6 GCPs is shown in figure 12.

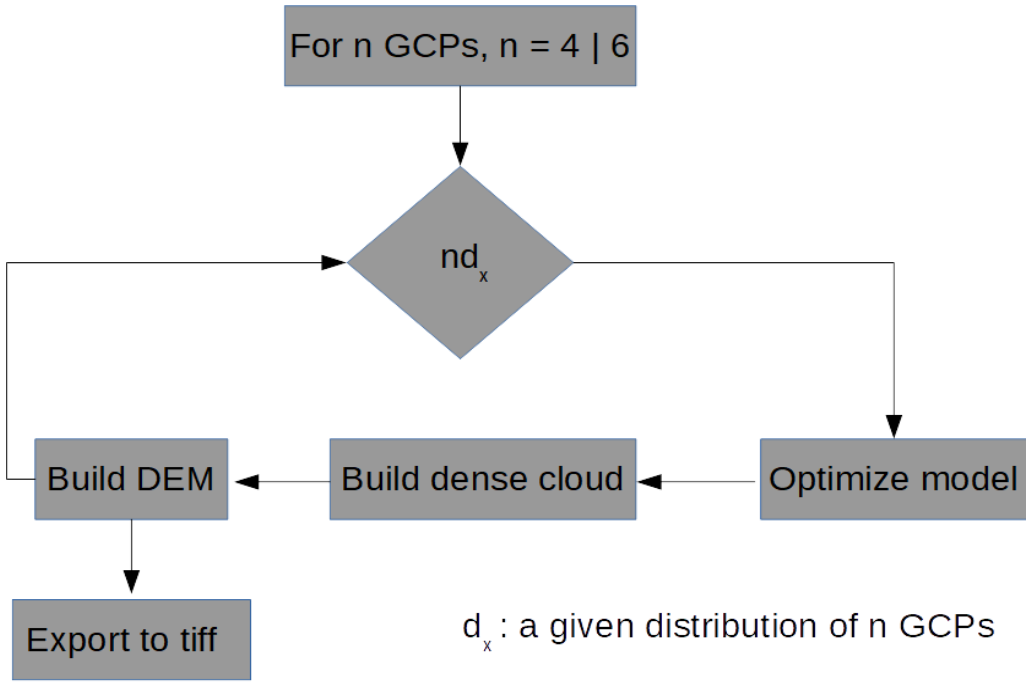

Figure 12. Creating DSMs based on different distributions of the same number of GCPs.

The obtained DSMs from both above steps and the reference GCPs were imported to QGIS[7]. The altitude of the GCPs were extracted from the DSMs, the altitude values collected and differences with the measured GCPs were analyzed.

3.3.3 Volume calculation

The area covered by UAV datasets collected at different heights will usually not be the same. In this study flight 2 covered the smallest area and flight 3 covered the largest area. To be able to compare the estimated volumes from a different DSMs, a common area from the DSMs used in volume calculations were selected.

[7] https://qgis.org/en/site/

4. Results

The day we started data collection was very misty. The recorded wind speed was less than 5 m/s. We designed the first flight session at a flight height of 30 meters, after checking the quality of the images, we decided to try a lower flight height, this time 20 meters. When we were ready to the third flight, the weather conditions were good enough to perform a flight at 40 meters height.

Data from three flight session collected the same day at three different height is processed using Agisoft PhotoScan with the same quality settings. Processing the steps required for creating DSMs takes approximately 7-10 hours on a machine with GPU, 64 GB RAM with 6 core running Microsoft Windows 10 Enterprise.

The general processing information for the three datasets is shown in table 2.

Table 2. General data attributes, number of UAV images, tie and dense cloud points from 3 flights

	Flight 2 (20 m)	**Flight 1 (30 m)**	**Flight 3 (40 m)**
Total number of photos	312	166	164
Used photos in data processing	234	163	164
Agisoft PhotoScan image quality > 0.5	226 (72%)	31 (19%)	164 (100%)
Tie points	283,784	82,251	163,854
Dense cloud points	302,208,788	164,999,843	164,379,892

The 8 GCPs, green represent control points and red are check points are shown in figure 13.

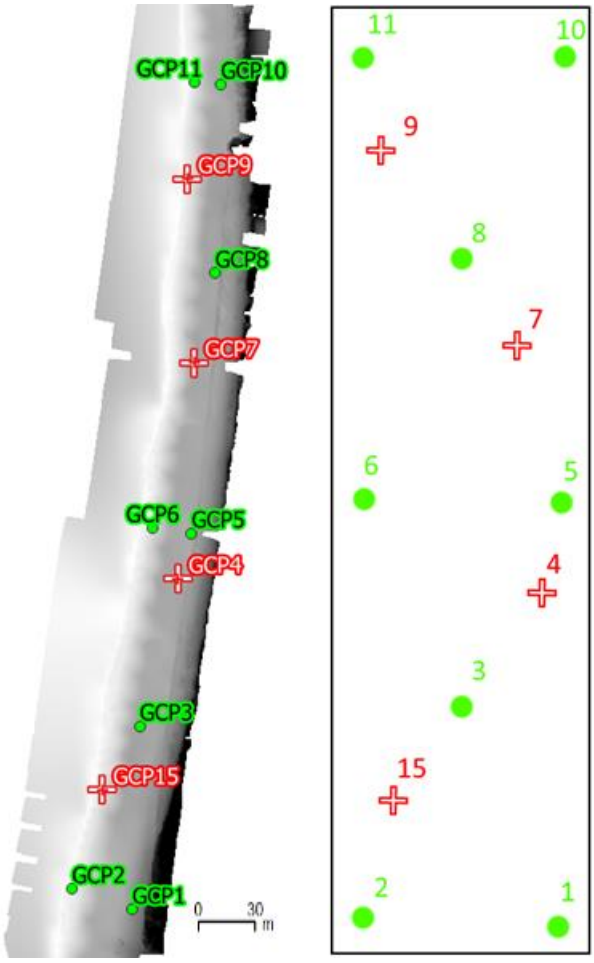

Figure 13. Control points (green dots) and check points (red crosses) on top of DMS from flight 2 and a rough drawing with approximate location of the GCPs. Approved for publication, LM2018/002559.

From the total numbers of 312, 166 images from flight 2 and 1 only 234, 163 were used in data processing, 6 images from flight 2 were excluded due to their blurriness, the rest of the images were excluded because they covered areas outside the study area or mainly contained water bodies. All the images from flight 3 were used in data processing. Since Agisoft PhotoScan succeeds in finding 82251 tie points from flight 1 images, all the 163 aligned images from flight 1 were used in DSM generation. Despite Agisoft PhotoScan's estimated low quality values, the final results do not record low quality DSMs from flight 1 images.

4.1 DSM quality assessment

The number and the distribution of the GCPs were designed before the flight sessions. 8 control points, defined to be used in the photogrammetric processes for creating the DSMs and 4 check points placed at different locations to be used to estimate the quality of the DSMs were measured by means of GNSS.

4.1.1 DSM quality in relation to GSD

DSM from the three flights using all 8 control points were produced with the same software settings. The obtained DSMs were loaded in QGIS and the estimated values of the check points were extracted from the DSMs, compared with the measured values, and standard deviation (STD) and Root Mean Square Error (RMSE) values were computed. The results shown in table 3 demonstrate the effect of pixel size on the quality of the produced DSMs, the RMSE of flight 3 is four times larger than flight 1 and 2; however, the difference between flight 1 and 2 is low, we have actually obtained lower STD and RMSE values in flight 1 with 30 meters flight height than flight 2 with 20 meters, this means that we can, under similar circumstances, save data collection and processing time by flying at 30 meters instead of 20 meters height.

Table 3. Standard deviation and root mean square error values for the three datasets using 8 GCPs.

Flights	Pixel size (cm)	STD (m)	RMSE (m)
Flight 3 (40 m)	1.51	0.102	0.088
Flight 1 (30 m)	1.14	0.020	0.018
Flight 2 (20 m)	0.79	0.021	0.018

The relation between flight height and the obtained STD and RMSE from table 2 is shown in a diagram in figure 20. It is expected that the absolute accuracy of the results will remain below the quality of the RTK-GPS measurements.

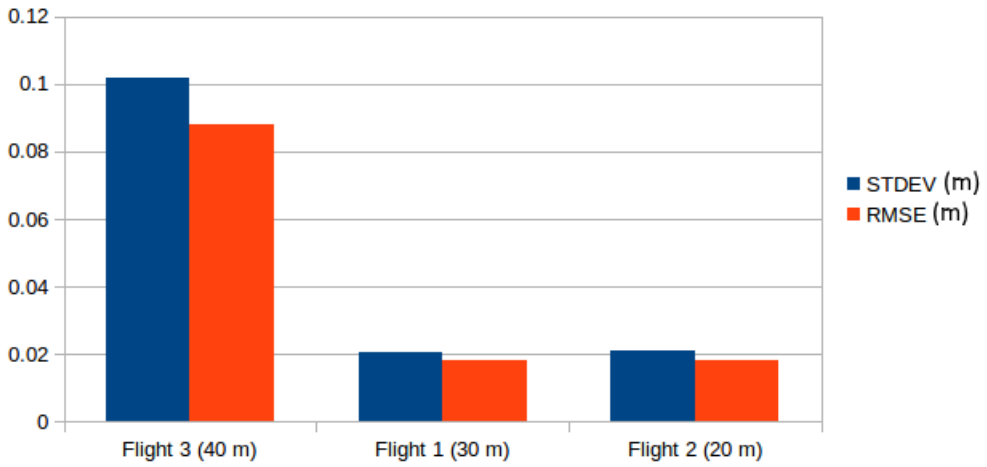

Figure 14. Standard deviation and root mean square error values for the three flights.

4.1.2 DSM quality in relation to number of GCPs

To study the effect of number of GCPs on the quality of the obtained DSMs, data from the three flight sessions were processed with the same GCPs, first with the four corner GCPs, then adding GCP5, GCP6, GCP3 and GCP8, see the location of the GCPs in figure 19.
Table 4 shows the selected combinations of GCPs and combination/distribution names that will be used throughout this document.

Table 4. Selected combinations of GCPs to study the relation between number of GCPs and DSM quality

GCP combination name	Selected GCPs
4GCPs	1, 2, 10, 11
5GCPs	4GCPs + 5
6GCPs	5GCPs + 6
7GCPs	6GCPs + 3
8GCPs	7GCPs + 8

The location of the GCPs used in the GCP combinations 5GCPs, 6GCPs and 7GCPs are shown in figure 21. The output of this part of the study was 15 DSMs, 5 for each flight session. The location of the check points was calculated from the obtained DSMs and the difference between the measured and the calculated values were computed. The RMSE values of the check points are given in table 5.

Table 5. Root Mean Square Error values using 4-8 GCPs to georeference the model and create DSMs

	RMSE (m)				
	4GCPs	**5GCPs**	**6GCPs**	**7GCPs**	**8GCPs**
Flight 3 (40 m)	0.445	0.148	0.107	0.108	0.088
Flight 1 (30 m)	0.450	0.104	0.035	0.018	0.018
Flight 2 (20 m)	1.238	0.031	0.029	0.034	0.018

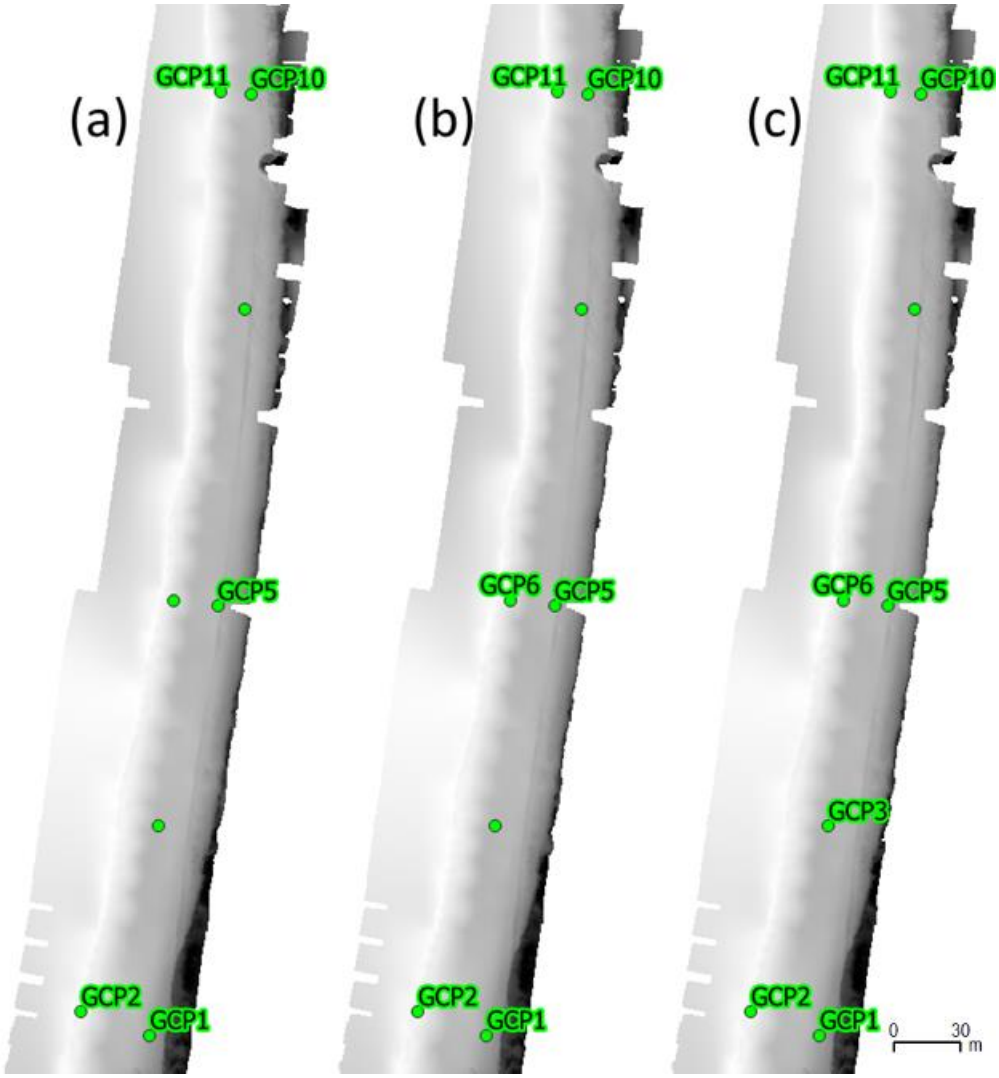

Figure 15. The labelled GCPs are used for georeferencing DSMs: 5GCPs, 6GCPs and 7GCPs. Approved for publication, LM2018/002559.

It is obvious from the results that the RMSE values decrease when more GCPs are used. When using only the four corner GCPs, the RMSE of flight 2 is three times the other two flights. Adding a single GCP, GCP5 at the middle of the area, the RMSE values are reduced by a factor of four in all the three flights, while the effect of more GCPs diminishes after GCP6. Figure 22 shows the relation between flight height, the number of GCPs and the obtained RMSE values.

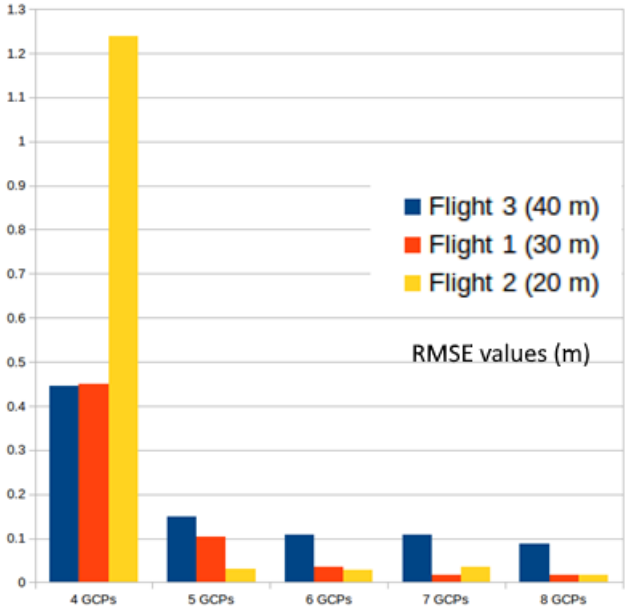

Figure 16. Root Mean Square Error values using 4, 5, 6, 7 and 8 GCPs for all the three flights.

4.1.3 DSM quality in relation to the distribution of GCPs

To further explore how the distribution of the GCPs influence the quality of the obtained DSMs, 3 combinations of 4 GCPs and 2 combinations of 6 GCPs from flight 2 were selected. The new GCP combinations/distributions were labelled as 4GCPs_D1, 4GCPs_D2 and 4GCPs_D3.

Testing different GCP distributions with 4 GCPs

The procedure defined in figure 12 were used to create 3 new DSMs with 3 different combinations of 4 GCPs. Figure 23 shows these 3 GCP combinations beside 4GCPs, which is the 4 corner GCPs used in the previous step.

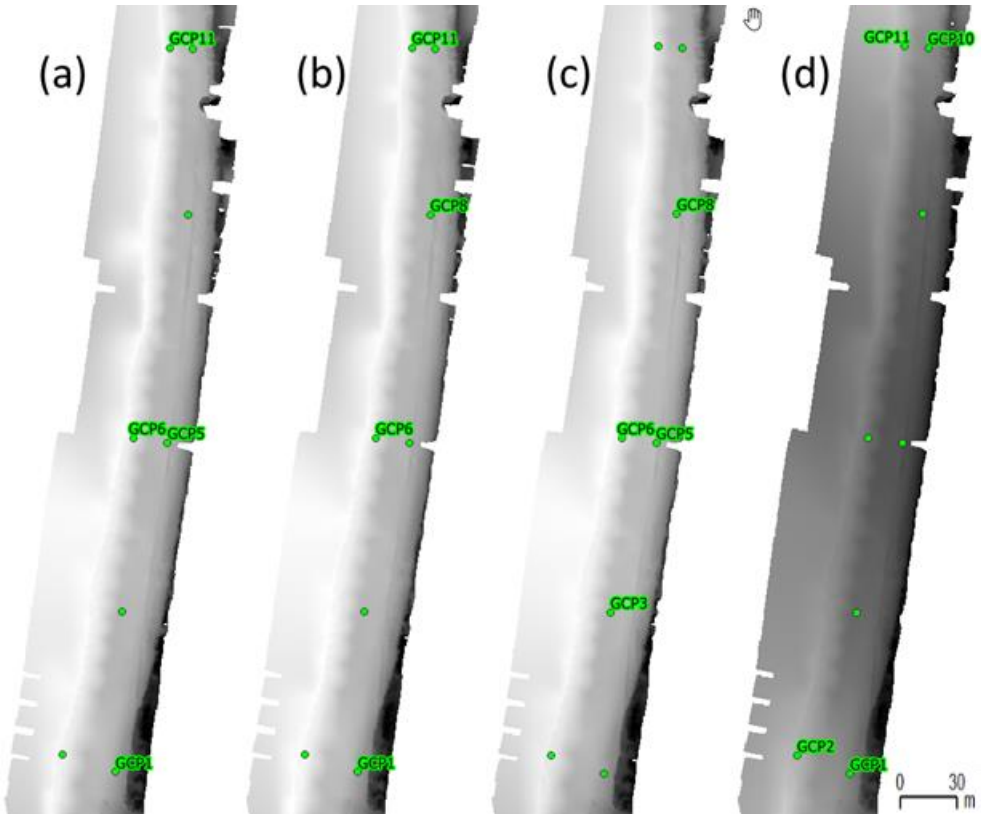

Figure 17. Four different distributions of 4 GCPs. (a) 4GCPs_D1, (b) 4GCPs_D2, (c) 4GCPs_D3 and (d) 4GCPs. Approved for publication, LM2018/002559.

The RMSE values of the control points obtained from DSMs created with 4 different distributions of 4 GCPs are shown in table 6 and figure 24.

Table 6. Root Mean Square Error obtained from different distributions of 4 GCPs.

Flight 2 (20 m)	Short name	RMSE (m)
DSM2 GCP (1, 5, 6, 11)	**4GCPs_D1**	**0.025**
DSM2 GCP (1, 6, 8, 11)	**4GCPs_D2**	**0.050**
DSM2 GCP (3, 5, 6, 8)	**4GCPs_D3**	**0.070**
DSM2 GCP (1,2,10,11)	**4GCPs (from previous step)**	**1.238**

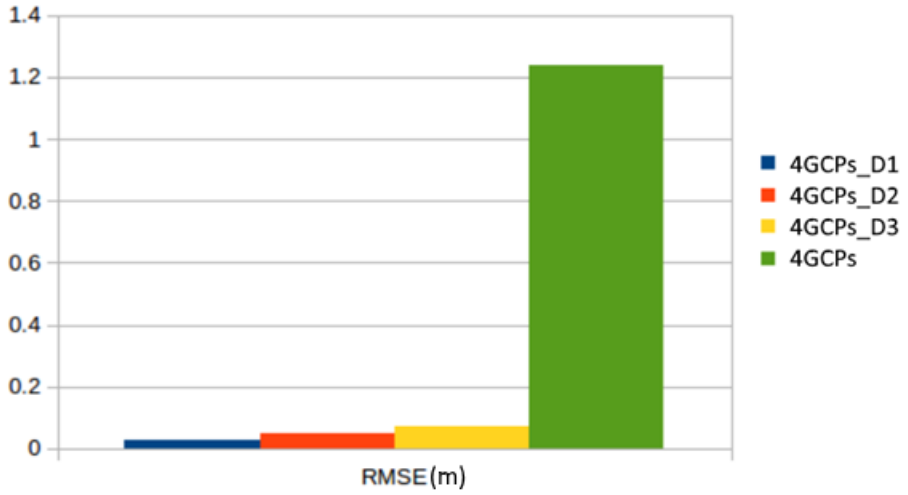

Figure 18. Root Mean Square Error values obtained from 4 GCPs in 4 different distributions.

It is interesting that the common rule of having GCPs at the corners of the study area results in the worst RMSE value compared to the other combinations, the other three results are quite close to each other; however, the best result is obtained where we use two GCPs at the middle of the area and one GCP at each end, i.e. the distribution 4GCPs_D1. The oblong shape of the study area has obviously influence on the best distribution of the GCPS.

Testing different GCP distributions with 6 GCPs:

Two DSMs with different combinations of 6 GCPs were created using the procedure from figure 12. The 2 new combinations are shown beside 6GCPs in figure 25.

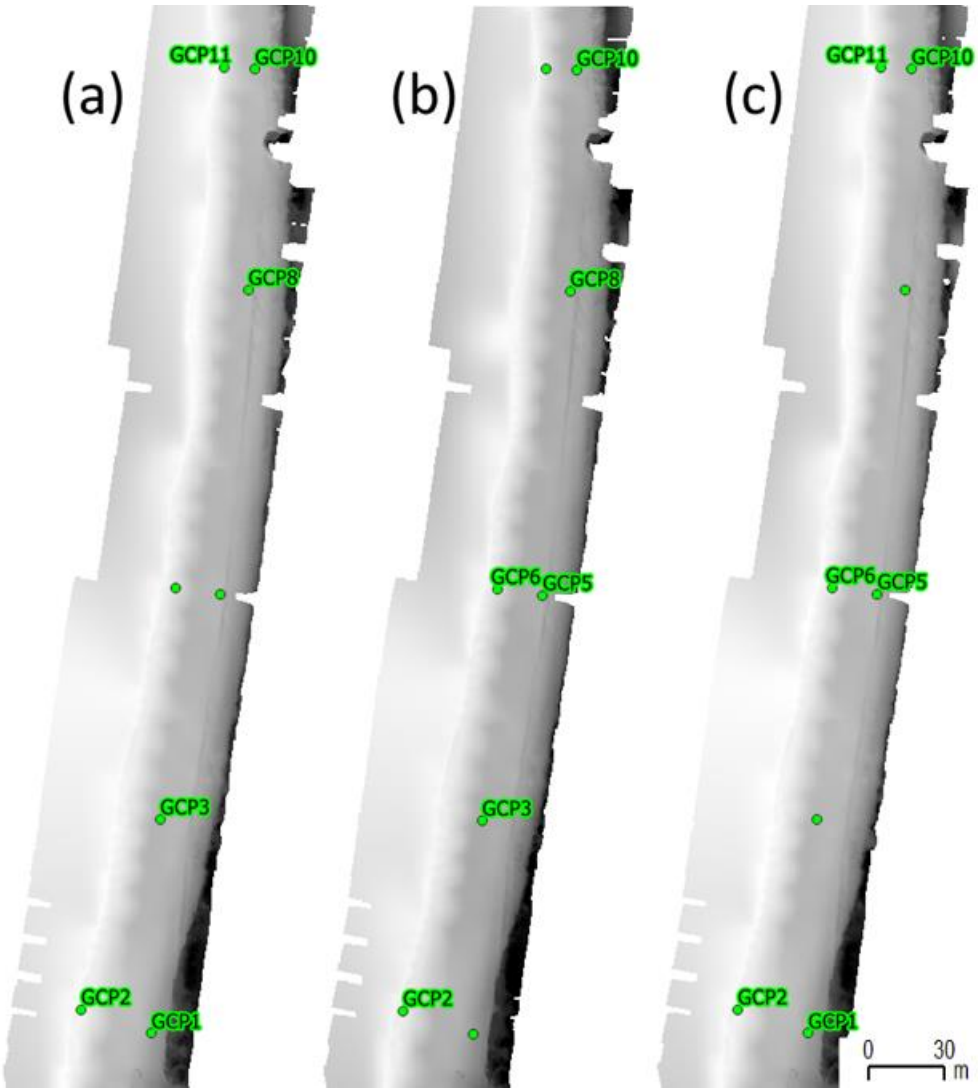

Figure 19. Three different distributions of 6 GCPs. (a) 6GCPs_D1, (b) 6GCPs_D2 and (c) 6GCPs. Approved for publication, LM2018/002559.

The RMSE values of the check points obtained from DSMs created with 3 different distributions of 6 GCPs are shown in table 7 and figure 26.

Table 7. Root Mean Square Error obtained from different distributions of 6 GCPs.

Flight 2 (20 m)	**Short name**	**RMSE (m)**
DSM2 GCP (1, 2, ,3 ,8 ,10, 11)	**6GCPs_D1**	**0.032**
DSM2 GCP (2, 3, 5, 6, 8, 10)	**6GCPs_D2**	**0.022**

DSM2 GCP (1, 2, 5, 6, 10, 11)	**6GCPs (from previous step)**	**0.029**

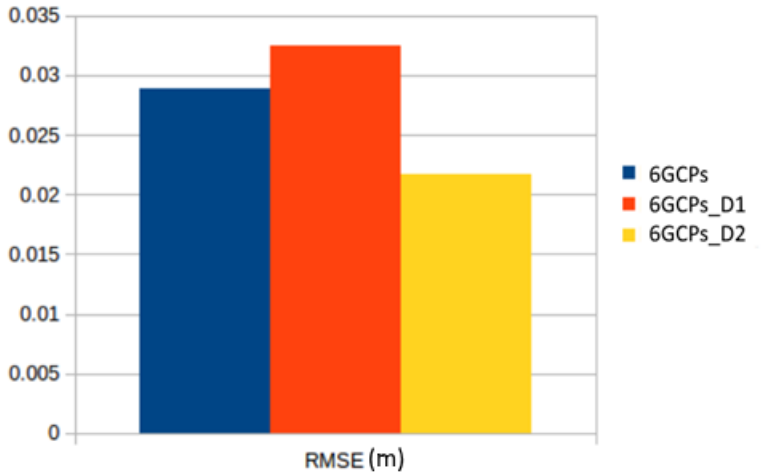

Figure 20. Root Mean Square Error values obtained from 6 GCPs in 3 different distributions.

Even though the results are similar, the same trend from 4 GCPs is repeated with 6 GCPs. The best result is not obtained by having two points at the ends and two at the middle of the area, but by distributing the GCPs so that we cover the study area best possible with the numbers of GCPs we have, 2 GCPs at the middle of the area and 2 distributed at each side of the area, in this case 6GCPs_D2.

Combining the RMSE values from 4 and 6 GCPs, we can see that the most accurate DSM from 4 GCPs has lower RMSE value than two of the DSMs georeferenced with 6 GCPs. This implies that the distribution of the points is more important than the number of the GCPs in some cases; however, more GCPs with the best distribution results in lowest RMSE. The best results from 4 and 6 GCP combinations are shown in figure 27.

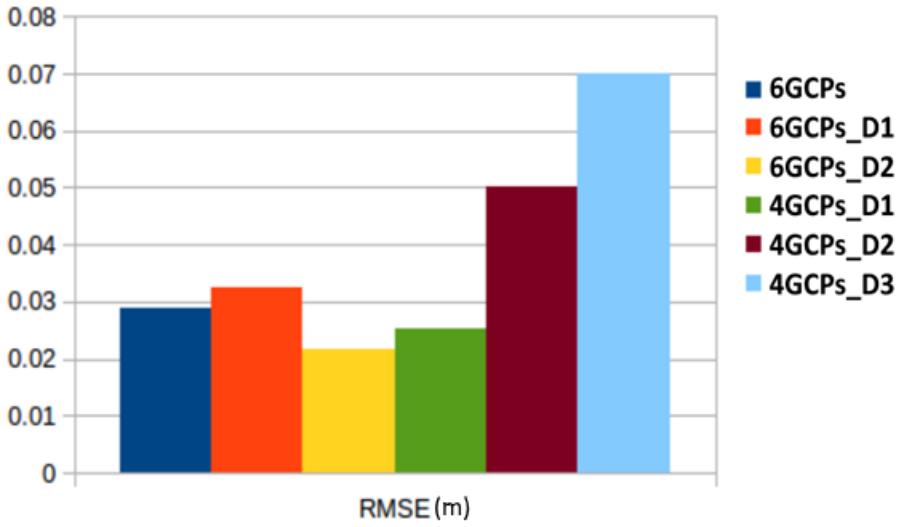

Figure 21. Comparing Root Mean Square Error values using 4 and 6 GCPs in different combinations.

4.1.4 Spatial distribution of the error

To analyze the spatial distribution of the errors, the area covered by the 8 GCPs was clipped and the difference between a number of the obtained DSMs georeferenced with different numbers of GCPs were computed. The results show that the low deviations are concentrated around the GCPs used in georeferencing the 3D models and the large deviations at the areas further away from GCPs.

The obtained DSM from a georeferenced model with 4 GCPs at the corners, i.e. 4GCPs deviates mainly with 5GCPs, in the middle of the study area, see figure 28 (a), while the difference between 4GCP_D1 and 4GCP_D3 that share GCP 5 and 6 in the middle of the study area, are largest at the corners. This indicates lower error values around the control points used in georeferencing the models. Distribution of the error between DSMs created from 4 and 5 control points are shown in figure 28.

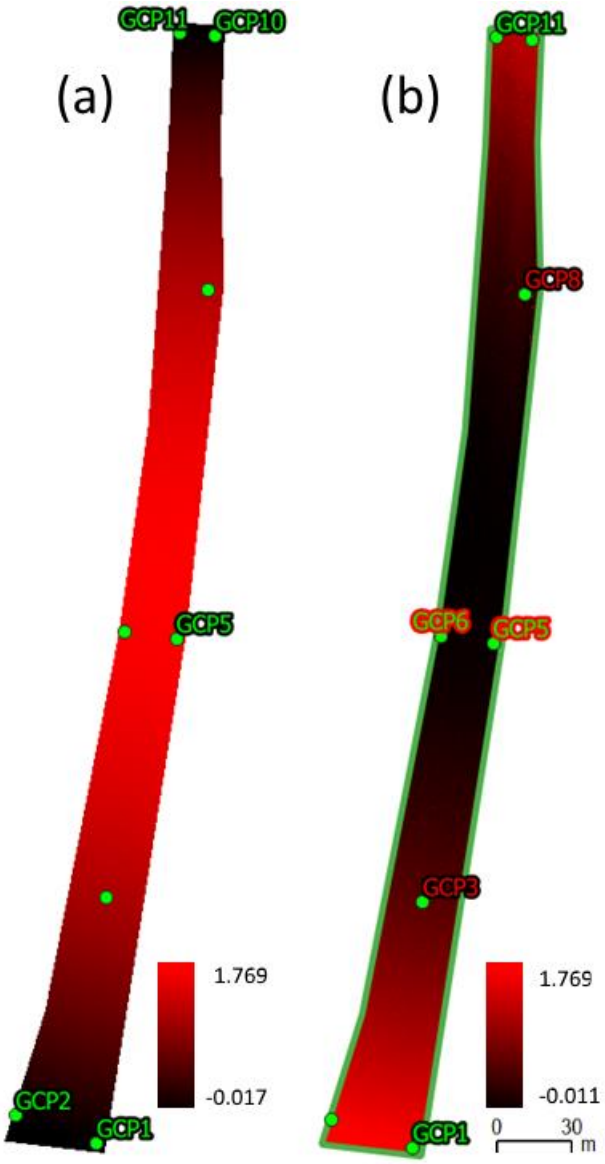

Figure 22, The difference between a DSM created using (a) 5GCPs and the 4 corner GCPS, (b) 4GCP_D1 and 4GCP_D3.

The differences between the DSMs created from 8, 6 and 4 GCPS show the same pattern. The results demonstrate a systematic deviation related to the number and the distribution of the GCPs. The distribution of the 6 GCPs in 6GCP_D3 results in a more homogeneous distribution of the error, while The DSM created with 7 GCPs records the largest deviation around the GCP that is not included in the processing, i.e. GCP 8.

Distribution of the errors between DSMs created from 8 GCPs and the best DSMs from 4 and 6 GCPs are shown in figure 29, the effect of GCP8 is clear in image (c).

Figure 23, The difference between the DSM created using all the 8 GCPs and the best DSMs from (a) 4 GCPs; 4GCP_D1 and (b) 6 GCPs; 6GCP_D3. image (c) is the difference between 8GCPs and 7GCPs

4.1.5 Overlapping images and DSM quality.

The number of overlapping images were investigated. The datasets contain an average of 7, 9 and 12 overlapping images for flight 2, 1 and 3 respectively at the location of the GCPs. The report created by Agisoft PhotoScan's "Survey Statistics" confirm the same result and demonstrate that the datasets do not contain areas with insufficient image overlap, successful implementation of SFM requires 2 or more photos (Nissen et al., 2016). Number of overlapping images for every GCP are shown in table 8.

Table 8. Number of overlapping images per GCP.

	Number of overlapping images per GCP							
GCP	1	2	3	5	6	8	10	11
Flight 2 (20m)	6	8	7	5	11	9	6	6
Flight 1 (30 m)	5	6	8	8	13	9	16	12
Flight 3 (40 m)	11	11	12	11	11	14	12	12

The large number of overlapping images in flight 3 do not result in a DSM with higher quality, this is mainly due to the large GSD value of flight 3. Camera locations and image overlap statistics are shown in figure 30. Comparing the quality of the GCPs from the same flight session shows that GCP6 from flight 1 with 13 overlapping images is the only GCP with an error at centimeter level, see table 9 in section 4.3.6.

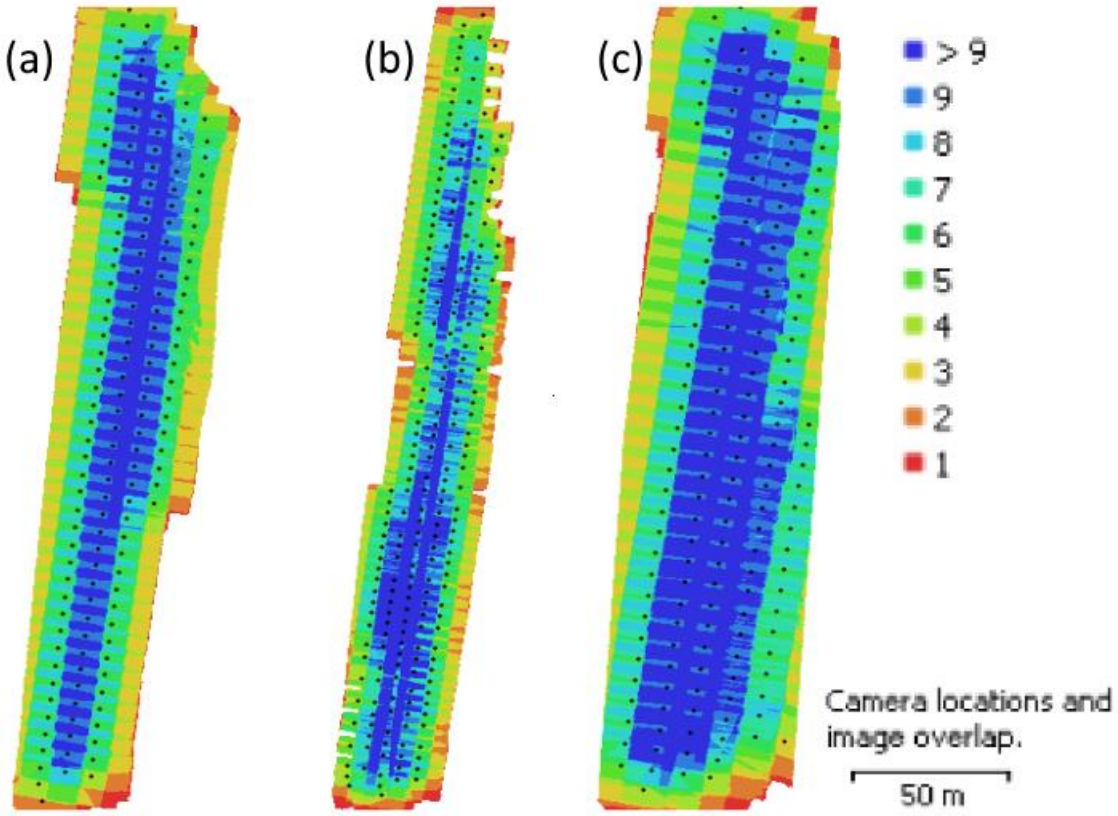

Figure 24. Image overlap statistics for flight (a) 1, (b)2 and (c) 3.

4.1.6 Land cover and DSM quality

The east side of the study area is covered by bushes and rocks, which results in more variation in the images. The size of the area covered by bushes and rocks in the datasets increases with flight height. The covered area by flight 2 at 20, flight 1 at 30 and flight 3 at 40 meters flight height are shown in figure 31.

Comparing the quality of the points close to the bushes and rocks with the ones in proximity to water, the results do not indicate any clear relation between the location and quality. The points GCP2, 6 and 11 which are the points most close to the water, have not registered a systematic reduced quality. Analyzing the quality of the GCPs used to georeferencing the models, flight 1 and 2 only have one point that exceeds the millimeter level, while 6 of the GCPs have an error greater than 1 cm in flight 3. The calculated values of the check points do not reflect any systematic relation to their locations, GCP 9 and 15 are the check points most close to the water side, se figure 32.

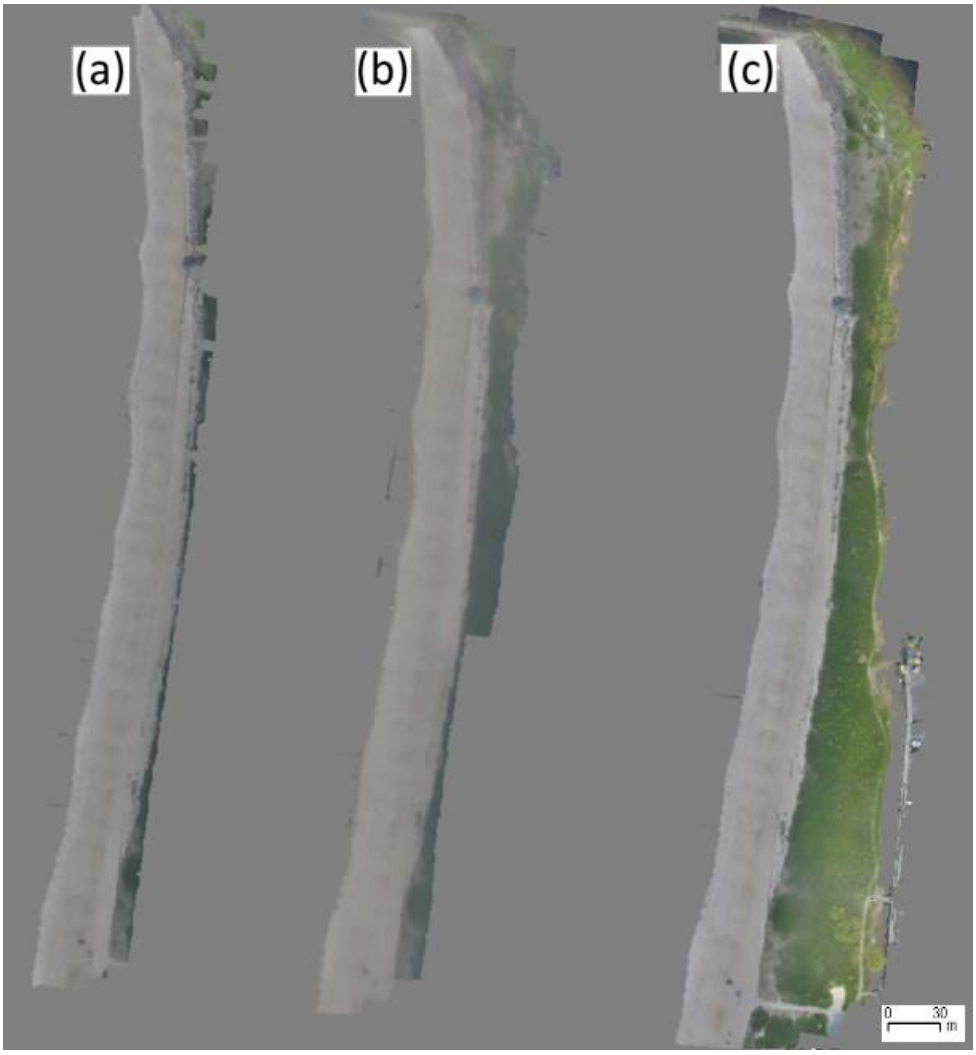

Figure 25. Land cover and the covered area by the three flights, (a) flight 2, 1 and 3. Approved for publication, LM2018/002559.

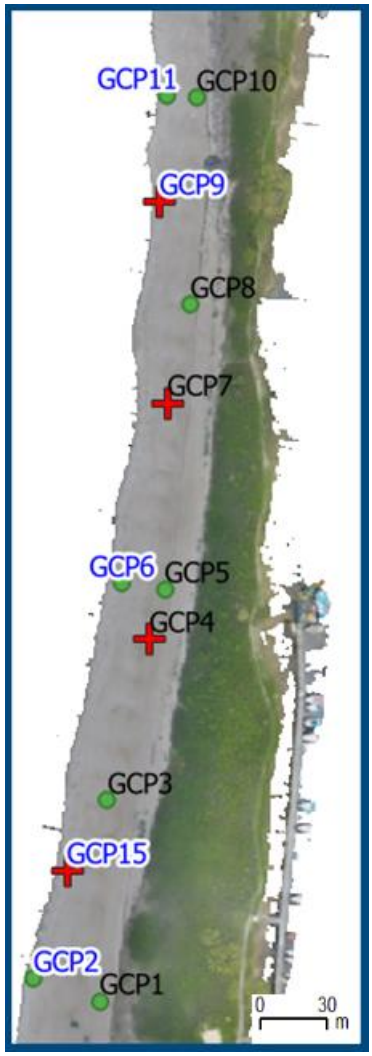

Figure 26. Near water GCPs are labelled blue on top of the orthomosaic from flight 3. Approved for publication, LM2018/002559.

The near water control points, i.e. GCP2, GCP6 and GCP11 and the near water check points, GCP15 and GCP9 are marked on top of the obtained orthomosaic from flight 3 in figure 32, water areas are shown in white since they are masked out from the UAV images.

The difference between measured and calculated elevation values of the 8 control points and the 4 check points for flight 3, 1 and 2 are shown in table 9 and 10.

Table 9. The difference between measured (M) and calculated elevation values from DSMs obtained by using 8GCPs, for 8 control points for flight 3, 1 and 2.

Name	M - DSM3 (m)	M - DSM1 (m)	M - DSM2 (m)
GCP1	-0.014	0.008	-0.015
GCP2	0.007	-0.006	-0.008
GCP3	-0.058	-0.008	0.004
GCP5	0.056	0.001	-0.010
GCP6	-0.027	0.014	-0.004
GCP8	-0.003	-0.003	-0.004
GCP10	-0.027	-0.004	0.001
GCP11	0.017	0.007	0.003

Table 10. The difference between measured (M) and calculated elevation values for 4 check points

GCP4	-0.018	-0.007	0.009
GCP7	-0.137	0.025	0.026
GCP9	0.099	-0.020	-0.005
GCP15	0.047	0.015	-0.024

4.1.7 DSM plane quality

The overall quality of the DSMs in the plane were measured by the RMSE values of Easting and Northing, the total errors of the models from Agisoft PhotoScan range between 1-2 cm; however, a quick investigation of the error values shows that GCP6 records of the largest dx and dy values in all three flights. Table 11 shows the max dx, dy and the RMSE values of Easting and Northing. Tables 12, 13 and 14 show the three model errors both in plane and height from Agisoft PhotoScan.

Table 11. Max GCP errors in plane

Flight	Max_dx (m)	Max_dy (m)	RMSEx (m)	RMSEy (m)
2	0.027 (GCP6)	0.016 (GCP2)	0.018	0.010
1	0.030 (GCP6)	0.027 (GCP6)	0.017	0.015
3	0.023 (GCP5)	0.017 (GCP6)	0.015	0.010

Table 12. Ground control point statistics. flight 3, 40 meters

Markers	East err. (m)	North err. (m)	Alt. err. (m)
GCP1	-0,004	-0,002	-0,003
GCP2	0,008	-0,007	-0,011
GCP3	0,008	0,01	0,048
GCP5	-0,023	0,015	-0,068
GCP6	0,017	-0,017	0,016
GCP8	-0,017	0,004	0,012
GCP10	-0,004	0,005	0,031
GCP11	0,021	-0,008	-0,034
RMSE	**0,015**	**0,01**	**0,035**

Table 13. Ground control point statistics. flight 1, 30 meters

Markers	East err. (m)	North err. (m)	Alt. err. (m)
GCP1	-0,011	0,008	-0,003
GCP2	0,009	-0,014	0,003
GCP3	-0,004	0,008	-0,002
GCP5	-0,002	0,022	0,004
GCP6	0,031	-0,027	0,001
GCP8	-0,007	0,002	-0,001
GCP10	-0,016	0,009	-0,001
GCP11	0,022	-0,007	0,001
RMSE	**0,017**	**0,015**	**0,002**

Table 14. Ground control point statistics. flight 2, 20 meters

Markers	East err. (m)	North err. (m)	Alt. err. (m)
GCP1	-0,016	0,005	0,002
GCP2	0,017	-0,016	0,004
GCP3	-0,004	0,008	-0,009
GCP5	-0,015	0,015	0,007
GCP6	0,028	-0,016	0,006
GCP8	-0,022	0,005	-0,007
GCP10	-0,0009	0,002	-0,003
GCP11	0,022	-0,001	0,005
RMSE	**0,018**	**0,01**	**0,005**

The quality of the obtained DSMs in the project is high with an, RMSE of less than 2 cm, when we take into account the time and the effort used to collect the data and produce the results. The accuracy obtained by using UAV matches or exceeds the accuracy obtained with the conventional aerial photography.

4.1.8 Sand volume estimates and DSM quality.

To be able to compare calculated volumes from the three flight sessions, a common extent that covered all the GCPs, from the best DSMs were clipped and volume calculations were computed. Figure 34 shows the clipped area, the 8 GCPs, the hillshade from flight 2, in grey, flight 1 in red and flight 3 in green.

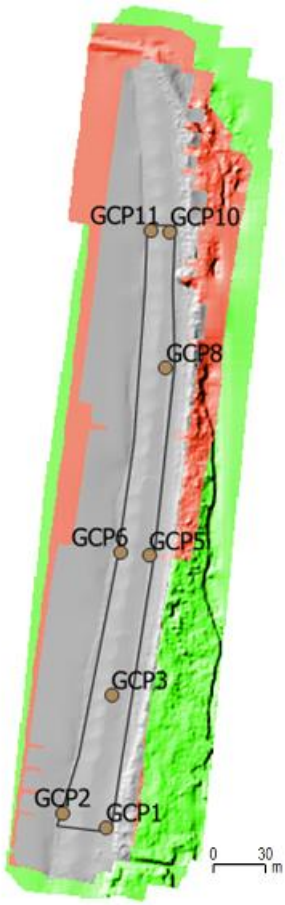

Figure 27. The common area from the three flights and the area used in volume calculations.

Volume calculations were carried out from the produced DSMs in QGIS. The volumes were calculated with the "Count Only Above Base Level" method, with base level assigned to 0.0. The calculated volumes are shown in table 15.

Table 15. Volume calculations

Flight	Volume (m^3)
2 (20 m)	11172
1 (30 m)	11189
3 (40 m)	11380

The difference between flight 3 and 2 is 191 m^3, i.e. more than ten times the difference between flight 2 and 1, which was computed to 17 m^3. The output of volume calculation confirms the same trend observed from the previous results when analysing the effect of GSD on the quality of the produced DSMs.

5. Discussions

This study shows that pixel size is important for the accuracy of the obtained DSMs. The different combinations of number and distribution of the GCPs verify that the number and the distribution of the GCPs have a large impact on the quality of the obtained DSMs. The results of the work confirm conclusions from other studies about the accuracy of UAV photogrammetry compared to Network RTK GPS (Barry and Coakley, 2015), stating that a vertical error of 1-3 GSD is expected for the correctly reconstructed model. Flight 1 and 2 have recorded a RMSE of 1.8 cm for GDS values of 0.79 and 1.14; however, flight 3, with a GSD of 1.51, results in a RMSE of 8.8 cm, when we were expecting a value less than 5 cm. The high RMSE value for flight 3 can also be seen in the statistics of the model, where large elevation errors at GCP3 and GCP5 were recorded, see Ground Control Point statistics from Agisoft PhotoScan in table 12. These two GCPs do not deviate from the rest of the GCPs in the other flights. We could try to reduce the error by locally adjusting the point cloud, but this has not been the intention of the study. Neither the quality of the images nor the number of the overlapping images explain the error in these two GCPs.

According to Pix4D (2018a), a minimum number of 5 GCPs is recommended, 5 to 10 GCPs are usually enough, even for large projects. More GCPs do not contribute significantly to increasing the accuracy. The results obtained from this project demonstrate that more than 5 GCPs will change the quality of the DSMs in different quantities depending on the pixel resolution. For instance, for UAV images with 1.51 cm GSD, the calculated RMSE values decreases from 14.8 to 10.7 and then to 8.8 cm when using 5, 6 and 8 GCPs, while UAV images with 0.787 cm GSD records high RMSE changes at 5 and 8 GCPs. It is important to mention that outputs from this study show that in some cases the distribution of the GCPs have higher impact on the accuracy than the number of GCPs. These results contradict recommendations from other experiences (PIX4D 2, 2018).

An important point in the relationship between pixel size, numbers of GCPs and the quality of DSMs is that the accuracy of the model created with 4 GCPs records the least accurate results in flight 2, the flight with the lowest flight height. The RMSE value is around three times larger than for the other two flights. The calculated values of the GCPs shows that the model is elevated twice as the other models, especially in the middle of the study area, where two of the check points are located, GCP4 and GCP7 and records the largest deviations. The relation between pixel size and number of GCPs changes this behaviour when using more GCPs.

The common recommendation of placing GCPs at the corners of the study area results in the highest RMSE values compared to the other combinations in this elongated study area. The best

results are obtained when having two GCPs in the middle of the area and other GCPs at each side. This combination of GCPs results in the best outputs both for 4 and 6 GCPs.

Distribution of the GCPs is related to the shape of the study area; this point must be taken into account when collecting UAV data for DSM generation. When exploring the number and the distribution of the GCPs, it is experienced that the distribution of the GCPs is important, the outcome of few number of GCPs with the best distribution will result in higher quality DSMs than larger numbers of GCPs lacking the optimal distribution. However, another important issue to be considered, when deciding number and distribution of GCPs, is the variation of the surface, more GCPs lead to more accurate reconstruction in areas with complex topography (PIX4D 1, 2018). More studies regarding distribution of GCPs both in plane and elevation are of great interest.

When analysing the quality of the obtained DSMs, it is interesting to check the relation between the location of the control points and the check points, for example to have an idea about the quality of the model outside the area covered by the control points, especially when the results of this study shows, that the best results are obtained from point distributions that do not create a closed area. Future works evaluating this point will be interesting.

It is expected that the absolute accuracy of any survey will remain lower than the accuracy of the measured GCPs used in the survey, therefore it is important to have the right consideration and expectation when planning UAV flights, It is important to measure the GCPs with a higher accuracy than the pixel size (Buczkowski, 2017). It is also important to be aware of the relationship between image pixel size and the size/width of the cross sign in the artificial GCPs, the larger the pixel size, the less is the accuracy of determining the central point of the GCP.

Despite Agisoft PhotoScan's low estimated quality values, all the aligned images from flight 1 were used. Future works comparing the results using only images with quality values above the recommended 0.5 will be interesting.

Assuming the availability of stable data-link connection in the study area, RTK GPS onboard UAVs would have advantages in this project since most of the images would have well corrected locations. Chen (2017) obtained elevation error of 1 GSD in open areas.

6. Conclusions

The results of the study show that pixel size affects the quality of the obtained DSMs, however, the difference between the quality of the produced DSMs from flight 1 and 2 is small, this means that, under similar circumstances as in this study, it is possible to fly at higher height to save data collection and processing time and still obtaining high quality results.

The number and the distribution of the GCPs are important parameters when georeferencing the model. The accuracy of the obtained DSMs is correlated to the number and the distribution of the GCPs. The combination 4GCPs_D1, with two points in the middle of the area and one at each of the ends, results in higher accuracy when the best result from 4 GCP and 6 GCP combinations are compared. This means that the distribution of the points has, in some cases, a stronger influence on the accuracy than the number of the GCPs, however, a larger number of GCPs with the best distribution results in lowest RMSE value.

Despite the misty weather at the time of flight 1 and the low number of images with high Agisoft PhotoScan quality values, the results from flight 1 are quite close to the obtained results from flight 2 and are much better than the results from flight 3, that has the largest number of overlapping images per GCP.

When analysing the relation between land cover and the quality of the check points, the study does not record any clear relation between the quality of the computed values and location of the calculated points, whether they are close to the bushes and rocks or located on the water side.

Creating digital elevation models have always been an expensive and time-consuming task and therefore have been one of the less updated GIS data sources. Using UAV images in DSM generation and the availability of both commercial and free open source software with the capability of processing images in a semi-automated way facilitate more frequently updated DSMs.

References

Agisoft LLC, Agisoft PhotoScan User Manual - 1.2 tech. rep, 2016.
http://www.agisoft.com/forum/index.php?topic=2179.0, Last accessed on 2018-11-07.
http://www.agisoft.com/forum/index.php?topic=1924.0, Last accessed on 2018-11-07.

Arango, C., Morales, C. A., Comparison between multicopter UAV and Total station for estimating stockpile volumes, 2015.

Buczkowski, A., How accurate is your drone survey? Everything you need to know. http://geoawesomeness.com/accurate-drone-survey-everything-need-know, Last accessed on 2018-11-07, 2017.

Casella, E., Rovere, A., Pedroncini, A. et al., Drones as tools for monitoring beach topography changes in the Ligurian Sea (NW Mediterranean), Geo-Mar Lett 36: 151. https://doi.org/10.1007/s00367-016-0435-9, 2016.

Chen, Lisa. Do RTK/PPK drones give you better results than using GCPs?, 2017.
https://pix4d.com/rtk-ppk-drones-gcp-comparison/, Last accessed on 2018-11-07.

eXtension, https://articles.extension.org/pages/40145/what-is-the-difference-between-a-recreational-grade-gps-a-mapping-grade-gps-and-a-survey-grade-gps, 2014.

Fonstad M. A., Marcus W. A., High resolution, basin extent observations and implications for understanding river form and process. Earth Surf Process Landf 35(6):680–698, 2010.

Goncalves, J.A., Henriques, R., UAV photogrammetry for topographic monitoring of coastal areas. ISPRS J. Photogrammetry Remote Sens. 104, 101–111, 2015.

Haala, N. and Rothermel, M. (2012) Dense Multi-Stereo Matching for High Quality Digital Elevation Models. PFG Photogrammetrie, Fernerkundung, Geoinformation Jahrgang, Heft 4, 331-343, 2012.

Haala, N., Rothermel, M., Dense Multiple Stereo Matching of Highly Overlapping Uav Imagery, International Archives of the Photogrammetry, Remote Sensing and Spatial Information Sciences, Volume XXXIX-B1, 2012.

Long, N., Millescamps, B., Pouget, F., Dumon, A., Lachaussée, N., and Bertin, X. ACCURACY ASSESSMENT OF COASTAL TOPOGRAPHY DERIVED FROM UAV IMAGES, Int. Arch.

Photogramm. Remote Sens. Spatial Inf. Sci., XLI-B1, 1127-1134, https://doi.org/10.5194/isprs-archives-XLI-B1-1127-2016, 2016.

Lowe, David G., Object Recognition from Local Scale-Invariant Features, Proceedings of the Seventh IEEE International Conference on Computer Vision, 1999.

Mancini, F.; Dubbini, M.; Gattelli, M.; Stecchi, F.; Fabbri, S.; Gabbianelli, G. Using Unmanned Aerial Vehicles (UAV) for High-Resolution Reconstruction of Topography: The Structure from Motion Approach on Coastal Environments. Remote Sens, 5, 6880-6898, 2013.

Mangor, Karsten, Human causes of coastal erosion. Available from http://www.coastalwiki.org/wiki/Human_causes_of_coastal_erosion, 2018, Last accessed on 2018-11-07

McGranahan, G., Balk, D. and Anderson, B., The rising tide: assessing the risks of climate change and human settlements in low elevation coastal zones', Environment and Urbanization, 19(1), pp. 17–37. doi: 10.1177/0956247807076960, 2007.

Nissen, E., Arrowsmith, J. Ramon, Crosby, C., Introduction to Structure-from-Motion, http://kb.unavco.org/kb/file.php?id=810, Last accessed on 2018-11-07, 2016.

PIX4D, Step 1. Before Starting a Project > 4. Getting GCPs on the field or through other sources (optional but recommended), https://support.pix4d.com/hc/en-us/articles/202557489-Step-1-Before-Starting-a-Project-4-Getting-GCPs-on-the-field-or-through-other-sources-optional-but-recommended-#gsc.tab=0, Last accessed on 2018-11-07, 2018a

PIX4D, Number and distribution of ground control points (GCPs) in corridor mapping, https://support.pix4d.com/hc/en-us/articles/202559299, Last accessed on 2018-11-07, 2018b

Raeva, P. L., Filipova, S.L., Filipov, D.G. Volume computation of a stockpile - A study case comparing GPS and UAV measurements in an open pit quarry. Int. Arch. Photogramm. Remote Sens. Spat. Inf. Sci., 41, 999–1004, 2016.

Snavely, N., Seitz, S.N., Szeliski, R., Modeling the world from internet photo collections. International Journal of Computer Vision 80, 189–210, 2008.

SONY, Interchangeable Lens Digital Camera A6000 Instruction Manual, (4-532-055-11)
Micasense. MicaSense RedEdge TM 3 Multispectral Camera User Manual tech. Rep., 1–27, May 2015.

Stalin, J. Leo, Gnanaprakasam, R. P. C., Volume Calculation from UAV based DEM, Vol 6, IJERT, International Journal of Engineering Research and Technology, https://www.ijert.org/phocadownload/V6I6/IJERTV6IS060076.pdf, 2017.

Turner, I. L., Harley, M. D., Drummond, C. D., UAVs for coastal surveying. Coast Eng. 114, 19–24, 2016.

Taveira-Pinto F., Silva R., Pais-Barbosa J., Coastal Erosion Along the Portuguese Northwest Coast Due to Changing Sediment Discharges from Rivers and Climate Change. In: Schernewski G., Hofstede J., Neumann T. (eds) Global Change and Baltic Coastal Zones. Coastal Research Library, vol 1. Springer, Dordrecht, 2011.

Westoby, M. J., Brasington, J., Glasser, N. F., Hambrey, M. J., & Reynolds, J. M., "Structure-from-motion" photogrammetry: A low-cost, effective tool for geoscience applications. Geomorphology, 179, 300–314. http://dx.doi.org/10.1016/j.geomorph. 2012.08.021, 2012.

Yoo, C. I. and Oh, T. S.: BEACH VOLUME CHANGE USING UAV PHOTOGRAMMETRY SONGJUNG BEACH, KOREA, Int. Arch. Photogramm. Remote Sens. Spatial Inf. Sci., XLI-B8, 1201-1205, https://doi.org/10.5194/isprs-archives-XLI-B8-1201-2016, 2016.

Zylka, A., Small Unmanned Aerial Systems (sUAS) for Volume Estimation, https://www.sensefly.com/app/uploads/2017/11/Small_Unmanned_Aerial_Systems_sUAS_for_ Volume_Estimation.pdf, 2014.

Series from Lund University

Department of Physical Geography and Ecosystem Science

Master Thesis in Geographical Information Science

1. *Anthony Lawther:* The application of GIS-based binary logistic regression for slope failure susceptibility mapping in the Western Grampian Mountains, Scotland (2008).
2. *Rickard Hansen:* Daily mobility in Grenoble Metropolitan Region, France. Applied GIS methods in time geographical research (2008).
3. *Emil Bayramov:* Environmental monitoring of bio-restoration activities using GIS and Remote Sensing (2009).
4. *Rafael Villarreal Pacheco:* Applications of Geographic Information Systems as an analytical and visualization tool for mass real estate valuation: a case study of Fontibon District, Bogota, Columbia (2009).
5. *Siri Oestreich Waage:* a case study of route solving for oversized transport: The use of GIS functionalities in transport of transformers, as part of maintaining a reliable power infrastructure (2010).
6. *Edgar Pimiento:* Shallow landslide susceptibility – Modelling and validation (2010).
7. *Martina Schäfer:* Near real-time mapping of floodwater mosquito breeding sites using aerial photographs (2010).
8. *August Pieter van Waarden-Nagel:* Land use evaluation to assess the outcome of the programme of rehabilitation measures for the river Rhine in the Netherlands (2010).
9. *Samira Muhammad:* Development and implementation of air quality data mart for Ontario, Canada: A case study of air quality in Ontario using OLAP tool. (2010).
10. *Fredros Oketch Okumu*: Using remotely sensed data to explore spatial and temporal relationships between photosynthetic productivity of vegetation and malaria transmission intensities in selected parts of Africa (2011).
11. *Svajunas Plunge:* Advanced decision support methods for solving diffuse water pollution problems (2011).
12. *Jonathan Higgins:* Monitoring urban growth in greater Lagos: A case study using GIS to monitor the urban growth of Lagos 1990 - 2008 and produce future growth prospects for the city (2011).
13. *Mårten Karlberg:* Mobile Map Client API: Design and Implementation for Android (2011).
14. *Jeanette McBride:* Mapping Chicago area urban tree canopy using color infrared imagery (2011).
15. *Andrew Farina:* Exploring the relationship between land surface temperature and vegetation abundance for urban heat island mitigation in Seville, Spain (2011).
16. *David Kanyari*: Nairobi City Journey Planner: An online and a Mobile Application (2011).

17. *Laura V. Drews:* Multi-criteria GIS analysis for siting of small wind power plants - A case study from Berlin (2012).
18. *Qaisar Nadeem:* Best living neighborhood in the city - A GIS based multi criteria evaluation of ArRiyadh City (2012).
19. *Ahmed Mohamed El Saeid Mustafa:* Development of a photo voltaic building rooftop integration analysis tool for GIS for Dokki District, Cairo, Egypt (2012).
20. *Daniel Patrick Taylor*: Eastern Oyster Aquaculture: Estuarine Remediation via Site Suitability and Spatially Explicit Carrying Capacity Modeling in Virginia's Chesapeake Bay (2013).
21. *Angeleta Oveta Wilson:* A Participatory GIS approach to *unearthing* Manchester's Cultural Heritage '*gold mine'* (2013).
22. *Ola Svensson:* Visibility and Tholos Tombs in the Messenian Landscape: A Comparative Case Study of the Pylian Hinterlands and the Soulima Valley (2013).
23. *Monika Ogden:* Land use impact on water quality in two river systems in South Africa (2013).
24. *Stefan Rova:* A GIS based approach assessing phosphorus load impact on Lake Flaten in Salem, Sweden (2013).
25. *Yann Buhot:* Analysis of the history of landscape changes over a period of 200 years. How can we predict past landscape pattern scenario and the impact on habitat diversity? (2013).
26. *Christina Fotiou:* Evaluating habitat suitability and spectral heterogeneity models to predict weed species presence (2014).
27. *Inese Linuza:* Accuracy Assessment in Glacier Change Analysis (2014).
28. *Agnieszka Griffin:* Domestic energy consumption and social living standards: a GIS analysis within the Greater London Authority area (2014).
29. *Brynja Guðmundsdóttir:* Detection of potential arable land with remote sensing and GIS - A Case Study for Kjósarhreppur (2014).
30. *Oleksandr Nekrasov:* Processing of MODIS Vegetation Indices for analysis of agricultural droughts in the southern Ukraine between the years 2000-2012 (2014).
31. *Sarah Tressel:* Recommendations for a polar Earth science portal in the context of Arctic Spatial Data Infrastructure (2014).
32. *Caroline Gevaert:* Combining Hyperspectral UAV and Multispectral Formosat-2 Imagery for Precision Agriculture Applications (2014).
33. *Salem Jamal-Uddeen:* Using GeoTools to implement the multi-criteria evaluation analysis - weighted linear combination model (2014).
34. *Samanah Seyedi-Shandiz:* Schematic representation of geographical railway network at the Swedish Transport Administration (2014).
35. *Kazi Masel Ullah:* Urban Land-use planning using Geographical Information System and analytical hierarchy process: case study Dhaka City (2014).
36. *Alexia Chang-Wailing Spitteler:* Development of a web application based on MCDA and GIS for the decision support of river and floodplain rehabilitation projects (2014).

37. *Alessandro De Martino:* Geographic accessibility analysis and evaluation of potential changes to the public transportation system in the City of Milan (2014).
38. *Alireza Mollasalehi:* GIS Based Modelling for Fuel Reduction Using Controlled Burn in Australia. Case Study: Logan City, QLD (2015).
39. *Negin A. Sanati:* Chronic Kidney Disease Mortality in Costa Rica; Geographical Distribution, Spatial Analysis and Non-traditional Risk Factors (2015).
40. *Karen McIntyre:* Benthic mapping of the Bluefields Bay fish sanctuary, Jamaica (2015).
41. *Kees van Duijvendijk:* Feasibility of a low-cost weather sensor network for agricultural purposes: A preliminary assessment (2015).
42. *Sebastian Andersson Hylander:* Evaluation of cultural ecosystem services using GIS (2015).
43. *Deborah Bowyer:* Measuring Urban Growth, Urban Form and Accessibility as Indicators of Urban Sprawl in Hamilton, New Zealand (2015).
44. *Stefan Arvidsson:* Relationship between tree species composition and phenology extracted from satellite data in Swedish forests (2015).
45. *Damián Giménez Cruz*: GIS-based optimal localisation of beekeeping in rural Kenya (2016).
46. *Alejandra Narváez Vallejo:* Can the introduction of the topographic indices in LPJ-GUESS improve the spatial representation of environmental variables? (2016).
47. *Anna Lundgren:* Development of a method for mapping the highest coastline in Sweden using breaklines extracted from high resolution digital elevation models (2016).
48. *Oluwatomi Esther Adejoro:* Does location also matter? A spatial analysis of social achievements of young South Australians (2016).
49. *Hristo Dobrev Tomov:* Automated temporal NDVI analysis over the Middle East for the period 1982 - 2010 (2016).
50. *Vincent Muller:* Impact of Security Context on Mobile Clinic Activities A GIS Multi Criteria Evaluation based on an MSF Humanitarian Mission in Cameroon (2016).
51. *Gezahagn Negash Seboka:* Spatial Assessment of NDVI as an Indicator of Desertification in Ethiopia using Remote Sensing and GIS (2016).
52. *Holly Buhler:* Evaluation of Interfacility Medical Transport Journey Times in Southeastern British Columbia. (2016).
53. *Lars Ole Grottenberg*: Assessing the ability to share spatial data between emergency management organisations in the High North (2016).
54. *Sean Grant:* The Right Tree in the Right Place: Using GIS to Maximize the Net Benefits from Urban Forests (2016).
55. *Irshad Jamal:* Multi-Criteria GIS Analysis for School Site Selection in Gorno-Badakhshan Autonomous Oblast, Tajikistan (2016).
56. *Fulgencio Sanmartín:* Wisdom-volkano: A novel tool based on open GIS and time-series visualization to analyse and share volcanic data (2016).

57. *Nezha Acil:* Remote sensing-based monitoring of snow cover dynamics and its influence on vegetation growth in the Middle Atlas Mountains (2016).
58. *Julia Hjalmarsson:* A Weighty Issue: Estimation of Fire Size with Geographically Weighted Logistic Regression (2016).
59. *Mathewos Tamiru Amato:* Using multi-criteria evaluation and GIS for chronic food and nutrition insecurity indicators analysis in Ethiopia (2016).
60. *Karim Alaa El Din Mohamed Soliman El Attar:* Bicycling Suitability in Downtown, Cairo, Egypt (2016).
61. *Gilbert Akol Echelai:* Asset Management: Integrating GIS as a Decision Support Tool in Meter Management in National Water and Sewerage Corporation (2016).
62. *Terje Slinning:* Analytic comparison of multibeam echo soundings (2016).
63. *Gréta Hlín Sveinsdóttir:* GIS-based MCDA for decision support: A framework for wind farm siting in Iceland (2017).
64. *Jonas Sjögren:* Consequences of a flood in Kristianstad, Sweden: A GIS-based analysis of impacts on important societal functions (2017).
65. *Nadine Raska:* 3D geologic subsurface modelling within the Mackenzie Plain, Northwest Territories, Canada (2017).
66. *Panagiotis Symeonidis*: Study of spatial and temporal variation of atmospheric optical parameters and their relation with PM 2.5 concentration over Europe using GIS technologies (2017).
67. *Michaela Bobeck:* A GIS-based Multi-Criteria Decision Analysis of Wind Farm Site Suitability in New South Wales, Australia, from a Sustainable Development Perspective (2017).
68. *Raghdaa Eissa*: Developing a GIS Model for the Assessment of Outdoor Recreational Facilities in New Cities Case Study: Tenth of Ramadan City, Egypt (2017).
69. *Zahra Khais Shahid*: Biofuel plantations and isoprene emissions in Svea and Götaland (2017).
70. *Mirza Amir Liaquat Baig*: Using geographical information systems in epidemiology: Mapping and analyzing occurrence of diarrhea in urban - residential area of Islamabad, Pakistan (2017).
71. *Joakim Jörwall*: Quantitative model of Present and Future well-being in the EU-28: A spatial Multi-Criteria Evaluation of socioeconomic and climatic comfort factors (2017).
72. *Elin Haettner*: Energy Poverty in the Dublin Region: Modelling Geographies of Risk (2017).
73. *Harry Eriksson*: Geochemistry of stream plants and its statistical relations to soil- and bedrock geology, slope directions and till geochemistry. A GIS-analysis of small catchments in northern Sweden (2017).
74. *Daniel Gardevärn:* PPGIS and Public meetings – An evaluation of public participation methods for urban planning (2017).
75. *Kim Friberg:* Sensitivity Analysis and Calibration of Multi Energy Balance Land Surface Model Parameters (2017).
76. *Viktor Svanerud:* Taking the bus to the park? A study of accessibility to green areas in Gothenburg through different modes of transport (2017).

77. *Lisa-Gaye Greene*: Deadly Designs: The Impact of Road Design on Road Crash Patterns along Jamaica's North Coast Highway (2017).
78. *Katarina Jemec Parker*: Spatial and temporal analysis of fecal indicator bacteria concentrations in beach water in San Diego, California (2017).
79. *Angela Kabiru*: An Exploratory Study of Middle Stone Age and Later Stone Age Site Locations in Kenya's Central Rift Valley Using Landscape Analysis: A GIS Approach (2017).
80. *Kristean Björkmann*: Subjective Well-Being and Environment: A GIS-Based Analysis (2018).
81. *Williams Erhunmonmen Ojo*: Measuring spatial accessibility to healthcare for people living with HIV-AIDS in southern Nigeria (2018).
82. *Daniel Assefa*: Developing Data Extraction and Dynamic Data Visualization (Styling) Modules for Web GIS Risk Assessment System (WGRAS). (2018).
83. *Adela Nistora*: Inundation scenarios in a changing climate: assessing potential impacts of sea-level rise on the coast of South-East England (2018).
84. *Marc Seliger*: Thirsty landscapes - Investigating growing irrigation water consumption and potential conservation measures within Utah's largest master-planned community: Daybreak (2018).
85. *Luka Jovičić*: Spatial Data Harmonisation in Regional Context in Accordance with INSPIRE Implementing Rules (2018).
86. *Christina Kourdounouli*: Analysis of Urban Ecosystem Condition Indicators for the Large Urban Zones and City Cores in EU (2018).
87. *Jeremy Azzopardi*: Effect of distance measures and feature representations on distance-based accessibility measures (2018).
88. *Patrick Kabatha*: An open source web GIS tool for analysis and visualization of elephant GPS telemetry data, alongside environmental and anthropogenic variables (2018).
89. *Richard Alphonce Giliba*: Effects of Climate Change on Potential Geographical Distribution of Prunus africana (African cherry) in the Eastern Arc Mountain Forests of Tanzania (2018).
90. *Eiður Kristinn Eiðsson*: Transformation and linking of authoritative multi-scale geodata for the Semantic Web: A case study of Swedish national building data sets (2018).
91. *Niamh Harty*: HOP!: a PGIS and citizen science approach to monitoring the condition of upland paths (2018).
92. *José Estuardo Jara Alvear*: Solar photovoltaic potential to complement hydropower in Ecuador: A GIS-based framework of analysis (2018).
93. *Brendan O'Neill*: Multicriteria Site Suitability for Algal Biofuel Production Facilities (2018).
94. *Roman Spataru*: Spatial-temporal GIS analysis in public health – a case study of polio disease (2018).
95. *Alicja Miodońska*: Assessing evolution of ice caps in Suðurland, Iceland, in years 1986 - 2014, using multispectral satellite imagery (2019).
96. *Dennis Lindell Schettini*: A Spatial Analysis of Homicide Crime's Distribution and Association with Deprivation in Stockholm Between 2010-2017 (2019).

97. *Damiano Vesentini*: The Po Delta Biosphere Reserve: Management challenges and priorities deriving from anthropogenic pressure and sea level rise (2019).
98. *Emilie Arnesten*: Impacts of future sea level rise and high water on roads, railways and environmental objects: a GIS analysis of the potential effects of increasing sea levels and highest projected high water in Scania, Sweden (2019).
99. *Syed Muhammad Amir Raza*: Comparison of geospatial support in RDF stores: Evaluation for ICOS Carbon Portal metadata (2019).
100. *Hemin Tofiq*: Investigating the accuracy of Digital Elevation Models from UAV images in areas with low contrast: A sandy beach as a case study (2019).